TAMPEREEN TEKNILLINEN YLIOPISTO
TAMPERE UNIVERSITY OF TECHNOLOGY

Jukka Viheriälä

Nanoimprint Lithography – A Next Generation Patterning Method for Nanophotonics

Julkaisu 891 • Publication 891

Tampere 2010

Tampereen teknillinen yliopisto. Julkaisu 891
Tampere University of Technology. Publication 891

Jukka Viheriälä

Nanoimprint Lithography – A Next Generation Patterning Method for Nanophotonics

Thesis for the degree of Doctor of Technology to be presented with due permission for public examination and criticism in Tietotalo Building, Auditorium TB103, at Tampere University of Technology, on the 15th of June 2010, at 12 noon.

Tampereen teknillinen yliopisto - Tampere University of Technology
Tampere 2010

ISBN 978-952-15-2364-9 (printed)
ISBN 978-952-15-2430-1 (PDF)
ISSN 1459-2045

Abstract

It is foreseen that nanoimprint lithography, NIL in short, will in the course of time have a strong impact on device applications which require precise and affordable nano-scale surface fabrication. My Thesis investigates NIL by applying it to various applications, while studying and solving a number of NIL-related physical and technological problems. When starting the work, the key challenge was to understand all the factors that could cause imprecision in the fabrication optical components. We expected that soft, and potentially nonprecise, stamps would prevent exact replication of functional components. However, we learned that with proper design of the stamp the precision of the stamp was very satisfactory.

Among many NIL methods available today, I decided to focus on a particular NIL version which relies on *soft stamps* in a regular mask aligner. I believe that soft UV-NIL will have a remarkable influence on nano-scale science because it is an affordable method to replicate nano-patterns on the wafer scale, despite the existence of other NIL methods which may have advantages over soft UV-NIL. The opportunity to utilize a mask aligner, the workhorse in every clean room for lithography, to replicate micro and nano-patterns in two and three dimensions is very tempting. I think that NIL using replicated soft stamps in a UV-mask aligner can make nano-pattering as accessible to everyone as the replication of micropatterns by means of photomasks and UV mask aligners.

For this Thesis, I have chosen several applications, including distributed feedback laser diodes, patterning and processing approaches of the top-down localization of indium arsenide quantum dots (QDs), patterning the facets of optical glass fibers, and preparing large-area nanoperforated membranes and membranous optical elements. I shall also discuss further development of high-aspect-ratio etching of gratings and report on novel etch results obtained for GaAs / AlGaAs and GaSb / AlGaSbAs material systems.

A major contribution in this Thesis to device fabrication was probably the development of an integratable, re-growth-free high performance laser where the grating was laterally coupled to the cavity field by applying soft UV-NIL to produce a strong resonance between the fundamental lasing mode and the grating.

My work on the top-down localization of InAs quantum dots and selective epitaxial growth was interesting because soft UV-NIL creates an extraordinary potential to prepare new materials and devices. I think that our work has been successful as to developing a soft UV-NIL technological platform, which yields precisely patterned growth-templates. I dare say that there is hardly any other lithography which could supply these templates to the same standard as soft UV-NIL.

One of the examples of the usefulness of NIL is the work in which we prepared a grating on a facet of an optical fiber; *i.e.*, an optical fiber element directly integrated into the fiber-end using a process that is easily amenable to volume production.

Our studies with membranes were driven by the need to develop a nano-sieve, which could be integrated into a silicon MEMS chip. Our study produced novel ways to make sturdy nano-perforated membranes, which were more than 3000 times wider than the thickness of the membrane. Finally, we demonstrated a novel way to integrate membranous optical elements with an optical fiber using a through-wafer via.

Acknowledgements

The work has been carried out at the Optoelectronics Research Centre (ORC) of Tampere University of Technology. I gratefully acknowledge the financial support of the Finnish agency for technology and innovation (TEKES), the European commission within the framework of FP7, the Finnish ministry of education, the Academy of Finland, the European space agency, the National graduate school for materials physics, the Ulla Tuominen foundation, the Foundation for Financial and Technical Sciences, the Finnish Foundation for Technical Promotion, and the Pirkanmaa Cultural Foundation.

I want also to express my gratitude to Emeritus Professor Markus Pessa for being my supervisor and supporting this thesis work. Without the work and many excellent ideas of Professor Tapio Niemi realization of this thesis would have been impossible. I also wish to acknowledge Dr. Mihail Dumitrescu for pushing NIL into new applications that have significantly contributed to this thesis. I also extend my gratitude toward Dr. Charis Reith who has contributed to this Thesis by editing the manuscript of the thesis and several of the publications.

My deepest gratitude goes to the excellent team members of the semiconductor processing group with whom it has been my pleasure to work. Without collaboration with M.Sc. Juha Tommila, M.Sc. Tuomo Rytkönen, Ms. Maija Karjalainen, Ms. Milla-Riina Viljanen, M.Sc. Jarkko Telkkälä, M.Sc. Juha Kontio, Dr. Pirjo Leinonen, M.Sc. Kimmo Harring, M.Sc. Pasi Pietilä, Dr. Changsi Peng and Mr. Aki Wallenius many of the developments over the past years would have been impossible. I also wish to extend my gratitude to all the members of the MBE group, simulation team and everyone working in the ultrafast and intense optics group. Especially I should acknowledge Dr. Antti Tukianen, Dr. Tomi Leinonen, M.Sc. Antti Laakso, Dr. Soile Suomalainen, M.Sc. Jari Lyytikäinen. M.Sc. Lauri Toikkanen, and Dr. Lasse Orsila, Dr. Matei Rusu, M.Sc. Samuli Kivistö, and Professor Oleg Okhotnikov for their help with practical issues related to semiconductors and optics. I certainly won't ever forget the all important contributions from M.Sc. Ilkka Hirvonen, Mr. Bengt Holmström and Mr. Timo Lindqvist in maintaining the instruments. Without seamlessly working facilities work in this field is very difficult. Of the people supplying us templates I wish to especially acknowledge the University of Joensuu physics department: Prof. Markku Kuittinen, Dr. Hemmo Tuovinen, Dr. Janne Laukkanen, M.Sc. Kari Leinonen, and M.Sc. Ismo Vartiainen.

Finally, I would like to thank my wife Kati, son Taavi, mother Eija, sister Taina and my closest relatives, for the support I have received over the years.

Contents

Abstract I
Acknowledgements III
Contents V
List of Publications VII
Author's Contribution IX
Related publications XI
Abbreviations and symbols XIII
1 Introduction 1
2 Lithography Techniques 5
2.1 Optical Lithography 5
2.2 Interference Lithography 6
2.3 Electron Beam Lithography 7
2.4 Nanoimprint lithography 8
2.5 State-of-the-art in NIL 15
3 Soft stamp UV-nanoimprint lithography 19
3.1 Fabrication of large-area templates 21
3.1.1 Large-area templates using special methods 23
3.2 Soft stamps 23
3.3 Anti-adhesion treatment 33
4 Pattern transfer using NIL 39
4.1 Residual layer etching 39
4.2 SiN mask layer 40
4.3 Pattern transfer with lift-off 41
4.4 Pattern transfer to compound semiconductor 43
4.4.1 GaAs/AlGaAs 44
4.4.2 InGaAs/InP material system 46
4.4.3 GaSb/AlGaSbAs material system 47
5 NIL in nanophotonics 49
5.1 Distributed feedback laser diodes 50

5.1.1 DFB lasers at 975 nm 56
5.1.2 DFB lasers at 894 nm 57
5.2 Nanopatterned templates for epitaxy 59
5.3 Nanopatterned membranes 63
5.3.1 Silicon-on- insulator based sieves 64
5.3.2 Silicon nitride-on-silicon based nanosieves 65
5.3.3 Membranous optical elements 67
5.4 Patterned facets of optical fibres 70
6 Conclusion 73
7 References 77

List of Publications

[P1] **Jukka Viheriälä**, Tuomo Rytkönen, Tapio Niemi and Markus Pessa (2008), Narrow linewidth templates for nanoimprint lithography utilizing conformal deposition, *Nanotechnology* , Volume 19, 015302, (7pp)

[P2] **Jukka Viheriälä**, Tapio Niemi, Juha Kontio, Tuomo Rytkönen and Markus Pessa (2007), Fabrication of surface reliefs on facets of single-mode-fibers using nanoimprint lithography, *Electronic Letters*, Volume 43, Number 3, pp. 150-152

[P3] **Jukka Viheriala**, Juha Tommila, Tomi Leinonen, Michail Dumitrescu, Lauri Toikkanen, Tapio Niemi and Markus Pessa (2009), Applications of UV-nanoimprint soft stamps in fabrication of single-frequency diode lasers, *Microelectronic Engineering*, Volume 86, Number 3, pp. 321-324

[P4] **Jukka Viheriälä**, Milla-Riina Viljanen, Juha Kontio, Tomi Leinonen, Juha Tommila, Mihail Dumitrescu, Tapio Niemi and Markus Pessa (2009), Soft Stamp UV-Nanoimprint Lithography for Fabrication of Laser Diodes, *Journal of Micro/Nanolithography MEMS, and MOEMS*, Volume 8, 033004

[P5] Lauri Sainiemi, **Jukka Viheriala**, Janne Laukkanen, Tapio Niemi and Sami Franssila (2009), Fabrication Of Silicon Membranes With Tunable Sized High Aspect Ratio Nanoperforations, Technical Digest of Transducers 2009, Paper M3.P045

[P6] **Jukka Viheriälä**, Tapio Niemi, Janne Laukkanen, Maija Karjalainen and Markus Pessa, Large area Nanoperforated SiN membranes for Optical and Mechanical Filtering (2010), *Microelectronics Engineering,* Volume 87, Number 5 - 8, pp. 1620-1622

[P7] Antti Tukiainen, **Jukka Viheriälä**, Tapio Niemi, Tuomo Rytkönen, Juha Kontio and Markus Pessa (2006), Selective growth Experiments on Gallium arsenide (100) surfaces patterned using UV-nanoimprint lithography, *Microelectronics Journal*, Volume 37, Issue 12, pp. 1477-1480

Author‘s Contribution

This thesis includes 7 papers published in open international literature. The Thesis also includes unpublished results, which are the result of my own work and cooperation with other researchers.

During the work I have worked in semiconductor processing, device packaging and device characterization. All facilities which supported this thesis were provided by the Optoelectronics Research Centre (ORC) at Tampere University of Technology.

My work for the nanofabrication at ORC has not been limited to research work presented in this thesis. Before the work with nanoimprint lithography, ORC's process know-how was limited to fabrication of patterns larger than 1 µm. To reach extreme linewidth (*i.e.* the one presented in paper P1) and fully fabricated devices containing nanopatterns, has required acquisition of new fabrication and metrology instruments, application of new methods and materials, definition of improved quality control mechanisms and hard work of several researchers, research assistants and technicians. I have led this technical development in my role as Head of the Semiconductor processing group. I have also supervised several MSc theses and started to supervise PhD students that will further enhance our nanofabrication and nanofabricated device expertise.

A list of my contributions in preparing scientific papers and experimental work is compiled in the Table below.

Paper #	Authors contribution in writing of the paper		Author's contribution in experimental work	
P1	Main author	90 %	Main work	80 %
P2	Main author	90 %	Main work	80 %
P3	Main author	80 %	Group work	50 %
P4	Main author	80 %	Group work	50 %
P5	Co-author	20 %	Group work	40 %
P6	Main author	90 %	Group work	50 %
P7	Co-author	30 %	Group work	50 %

Related publications

[1] **Jukka Viheriälä**, Tapio Niemi, Juha Kontio and Markus Pessa (2010), Nanoimprint Lithography - Next Generation Nanopatterning Methods for Nanophotonics Fabrication, *Recent Optical and Photonic Technologies*, Ki Young Kim (Ed.), ISBN: 978-953-7619-71-8, INTECH, pp. 275 – 298, Available from: http://sciyo.com/articles/show/title/nanoimprint-lithography-next-generation-nanopatterning-methods-for-nanophotonics-fabrication

[2] Lauri Sainiemi, **Jukka Viheriälä**, Tiina Sikanen, Janne Laukkanen and Tapio Niemi (2009), Versatile nanoperforated silicon membranes for filtering applications, Accepted for publication in Journal of Micromechanics and Microengineering

[3] Antti Laakso, Mihail Dumitrescu, **Jukka Viheriälä**, Jukka Karinen, Mikko Suominen And Markus Pessa (2009), Optical modeling of laterally-corrugated ridge-waveguide gratings, *Opt. Quantum Electron.*, Volume 40, pp. 907-920

[4] Antti Laakso, Mihail Dumitrescu, **Jukka Viheriälä,** Jarkko Telkkälä, Juha Tommila, Kimmo Haring, Tomi Leinonen, Sanna Ranta and Markus Pessa (2009), Laterally-corrugated ridge-waveguide distributed feedback lasers at 980 nm, *Opt. Quantum Electron.*, Volume 41, pp. 11-16

[5] **Jukka Viheriälä**, Milla-Riina Viljanen, Juha Kontio, Tomi Leinonen, Juha Tommila, Mihail Dumitrescu, Tapio Niemi, Markus Pessa (2009), Soft Stamp UV-Nanoimprint Lithography for Fabrication of Laser Diodes, Published in *SPIE proceedings*, Volume 7271, pp. 72711O-72711O-10

[6] **Jukka Viheriälä**, Antti Laakso, Mihail Dumitrescu, Juha Tommila, Kimmo Haring, Tomi Leinonen, Sanna Ranta, Markus Pessa (2009), Surface-grating-based distributed feedback lasers fabricated using nanoimprint lithography, Published in *IEEE Proceedings*, Vol 1, p. 95-98, ISBN 978-1-4244-2004-9

[7] Brian K Canfield, Hannu Husu, Juha Kontio, **Jukka Viheriälä**, Tuomo Rytkönen, Tapio Niemi, Eric Chandler, Alex Hrin, Jeff A. Squier and Martti Kauranen (2008), Inhomogeneities in the nonlinear tensorial responses of arrays of gold nanodots, *New J. Phys.*, Volume 10, 013001

[8] Martti Kauranen, Hannu Husu, Sami Kujala, Brian K. Canfield, Janne Laukkanen, Benfeng Bai, Markku Kuittinen, Jari Turunen, Juha Kontio, **Jukka Viheriälä**, Tapio Niemi, Eric Chandler, Jeff A. Squier (2008), Role of local fields and defects in the nonlinear response of metal nanostructures, Published in *SPIE proc.*, Volume 7032, pp. 70321J-1 - 70321J-10

[9] Jian Lin, Mika Lindén, Jussi Pekkanen, **Jukka Viheriälä**, Matti Mäntysalo, and Ronald Österbacka (2009), High-resolution inkjet printing utilizing easy-processing surface energy pattern, Submitted to *Advanced Materials*

[10] Nikolai V. Tkachenko, Vladimir Chukharev, Petra Kaplas, Antti Tolkki, Kimmo Haring, **Jukka Viheriälä**, Tapio K. Niemi, Helge Lemmetyinen (2010), Resistivity of Thin Organic Films, *Applied Surface Science*, Volume 256, pp. 3900-3905

[11] J. Pozo, J. Hu, J.M. Rorison, Mika Saarinen, Janne Konttinen, **Jukka Viheriälä**, Pirjo Leinonen, Tomi Jouhti, Markus Pessa (2006), Improvements in GaInNAs/GaAs Quantum Well Lasers using Focused ion-beam post-processing, Published in *SPIE proceedings*, Volume 6184, pp. 61840B-1-61840B-10

[12] J. Pozo, N. Vogiatzis, J.W. Lu, O. Ansell, J.M. Rorison, P.J. Heard, Pietari Tuomisto, Janne Konttinen, Mika Saarinen, Changsi S. Peng, **Jukka Viheriälä**, Tomi Leinonen, Markus Pessa M. (2008)., Fabrication and characterization of GaInNAs/GaAs semiconductor optical amplifiers, Published in *SPIE proc*eedings, Volume 6997, pp. 69970C-69970C-9

[13] Y.N. Qiu, G. Papaioannou, J. Pozo, J.M. Rorison, Mika Saarinen, Janne Konttinen, **Jukka Viheriälä**, Pirjo Leinonen, Tomi Jouhti, Markus Pessa (2008), Ion irradiation induced nitrogen mobility in a GaInNAs quantum well laser, *Semicon. Sci. Tech.* 23, Volume 1-5, 075028 (5pp)

[14] Antti Tukiainen, Lauri Toikkanen, Matti Haavisto, Vesa Erojärvi, Ville Rimpiläinen, **Jukka Viheriälä**, Markus Pessa (2006), AlInP / AlGaInP quantum well lasers grown by molecular beam epitaxy, *IEEE Photon. Tech. Lett.*, Volume 18, pp. 2257-2259

Abbreviations and symbols

AFM	Atomic force microscope
ALD	Atomic layer deposition
BOX	Buried oxide
CTE	Coefficient of thermal expansion
CW	Continuous wave
DFB	Distributed feedback
DFB-LD	Distributed feedback laser diode
EBL	Electron beam lithography
FDTS	Perfluorodecyltrichlorosilane
h-PDMS	Hard polydimethylsiloxane
IC	Integrated circuit
ICP	Inductively coupled plasma
m	Order of a grating
n_{eff}	Effective refractive index of a waveguide
NIL	Nanoimprint lithography
ORC	Optoelectronics Research Centre
PDMS	Polydimethylsiloxane
PECVD	Plasma enhanced chemical vapor deposition
PMMA	Poly(methyl methacrylate)
QD	Quantum dot
RIE	Reactive ion etching
SEM	Scanning electron microscope
SiN	Silicon nitride[(1)]
SMSR	Side-mode suppression-ratio

[(1)] Often SiN referees to non-stoichiometric SiN (compare to Si_3N_4).

SOI	Silicon on insulator
TTV	Total thickness variation
TWV	Through-wafer via
Λ	Period
λ	Wavelength
κ	Coupling coefficient

1 Introduction

Nanophotonics is a wide research field that covers many interesting areas of applications, branching from cutting-edge science, including plasmonics, metamaterials and cavity quantum electrodynamics in high-Q cavities, all the way to applied sciences, such as silicon nanophotonics for on-chip optical interconnections and single-frequency semiconductor light sources. Many practical devices utilize nanopatterned surfaces which consist of nanoscopic gratings, photonic crystals, waveguides and metal structures.

There exist wonderful demonstrations of nanotechnology-based lasers and other photonic components. However, difficult questions related to the fabrication need be addressed before such components enter the market. Demonstrations in the scientific literature have largely relied heavily on the use of direct writing lithographic methods, such as electron beam lithography or focused ion beam lithography. These methods, although excellent for scientific studies, cannot be scaled up to allow cost-effective production of nanophotonics. Lithographic solutions developed for integrated circuits can produce extremely narrow linewidths and deliver high precision but are difficult to transfer to photonics fabrication.

Since the introduction of nanoimprint lithography (NIL) in 1995 (Chou *et al*. 1995), there has been widespread interest in the development of NIL for various applications. As early as 2003 NIL had gained substantial support and was chosen as one of MIT's Technology Review's "10 Emerging Technologies That Will Change the World" (Technology Review 2003). The selection was justified by the fact that NIL can bridge the gap between lab level nanotechnology research and production level manufacturing requirements.

I also saw the potential of NIL and when ORC acquired a new UV - mask aligner from EV Group (EVG) in early 2007; the aligner was equipped with special tools that allow NIL. In principle, modifications to the regular mask aligner are rather small. The mask holder is replaced with a transparent vacuum chuck and the wafer chuck is replaced by a special wafer

chuck for NIL. The tooling was designed to be used for imprinting 3″ substrates, but it could also be used for smaller samples. The change from NIL-mode to UV mask aligner mode can be made in one minute.

With the mask aligner we decided to use soft stamps because they enable large area imprinting with low pressure (25 to 850 mbar) available from the tool (Plachetka *et al.* 2004). An additional benefit of the soft material is its robustness against small defects, such as particles. However, through the years we worked with NIL we often found ourselves in the situation where we required the precision offered by hard materials and the process robustness offered by soft materials. This is one of the tradeoffs one faces when working with NIL. Deformation of the stamp enables uniform contact but reduces the quality of the replica. We tackled the problem by developing our own stamps, having relatively hard surfaces but simultaneously allowing conformal imprinting due to their flexibility, even on the microscale. It was also possible to engineer stamps softness, as discussed later. Our stamps allowed precise patterning over full wafers (2″ and 3″) and we believe that also larger wafers could be imprinted with the same stamp concept, if needed.

A major contribution in this Thesis to device fabrication was probably the development of an integratable, re-growth-free high performance laser where the grating was laterally coupled to the cavity field applying soft UV-NIL to produce a strong resonance between the fundamental lasing mode and the grating. For this work NIL should be able to imprint 3″ wafers at good enough pattern registration for 0.5 µm overlay accuracy. This means that patterns can not contract or stretch (laterally across the wafer) more than 6.5 ppm during the replication process. Additionally patterns should not have any irregularities across the laser cavity because imperfections would ruin the operation of the feedback grating. A linewidth requirement of 200 nm was enough for realization of third order gratings and the linewidth for first order gratings was in the range between 50 nm and 100 nm. In addition the application required very high-aspect-ratio nanoetching. This we studied extensively for the main material systems of interest.

My work on the top-down localization of InAs quantum dots (QDs) and selective epitaxial growth was interesting because soft UV-NIL creates an extraordinary potential to prepare new materials and devices. I think that our work has been successful with regard to developing a soft UV-NIL technological platform, which yields precisely patterned growth-templates. I dare say

that there is hardly any other lithography which could supply these templates to the same standard as soft UV-NIL. Here, full 2″-wafer ought to be imprinted at very high resolution (sub-50 nm linewidth). Even though this work was purely basic research, more than one hundred different wafers were imprinted over the years for various experiments.

One of the examples of the usefulness of NIL is experiment for which prepared a grating on a facet of an optical fiber; *i.e.*, an optical fiber element directly integrated into the fiber-end using a process that is easily amenable to volume production. This application is a good example that imprint lithography could be applied to areas that are normally out of reach for other volume fabrication methods. If a surface is accessible, it is probably possible to imprint it with nanopatterns.

Our studies with membranes were driven by the need to develop a nano-sieve, which could be integrated into a silicon MEMS chip. Our study produced novel ways to make sturdy nano-perforated membranes, which were more than 3000 times wider than the thickness of the membrane. Finally, we demonstrated a novel way to integrate membranous optical elements with an optical fiber using the through-wafer via.

2 Lithography Techniques

In this Section I briefly review state-of-the-art lithographic methods and introduce nanoimprint lithography as a cost-effective method for nanophotonics applications. In Section 3 I shall introduce soft UV-NIL, an imprint method using soft and flexible stamps, as a method for patterning compound semiconductor optoelectronics. Finally, in Sections 4 and 5 I shall highlight some of the NIL applications and pattern transfer results.

2.1 Optical Lithography

The era of microlithography started to develop in the 1970's. It was driven mainly by the development of integrated circuits (ICs). This industry created a need for high volume, perfect replication of ever smaller patterns on a substrate, at minimal costs. The main method to achieve this was, and still is, optical lithography. This branch of lithography utilizes templates, also known as photomasks, having transparent and opaque areas. Light is shone through the photomask on a substrate which is coated with a photosensitive thin film called a photoresist. Photoresist areas that are exposed to light will transform to either soluble or insoluble to the photoresist developer. If exposure makes photoresist soluble it is called positive photoresist and *vice versa* if photoresist becomes insoluble it is called negative photoresist. Light replicates the patterns from the photomask to the photosensitive film, and further steps are taken to transfer the copied patterns to the substrate. In the early 1970's, the required dimensions for the ICs ranged from 2 µm to 5 µm. Replication of these patterns was simply achieved by using mercury-arc based UV-light and bringing the photomask and the substrate in close proximity or into contact during the exposure. Systems based on this operation principle are still used today in microfabrication, due their simplicity, low cost, high throughput and good process quality. These systems, called UV-contact mask aligners, reach resolutions from a few micrometers to the sub-half-micron level, depending on the exposure wavelength and the contact method. With fully automated systems the throughput can exceed 100 wafers per hour (wph) and reach an overlay accuracy of 0.25 µm (Suss 2009).

An ever increasing demand for smaller and smaller linewidths has demanded more complex exposure systems. Nowadays, state-of-the-art systems in IC production reach 32 nm linewidths by using deep-UV ArF-light sources at 193 nm wavelength and exposing patterns using immersion scanners, phase shift masks and double exposure schemes. Exposure is based on an image reduction technique that projects the photomask onto the substrate and simultaneously reduces the size of the patterns many times. This allows the photomasks to be fabricated with looser tolerances than the final pattern. These systems are also very productive and able to pattern more than one hundred and fifty 300-mm wafers per hour and to reach better than 2.5 nm alignment between subsequent patterning steps (ASML 2009).

These exposure systems, reaching 45 nm or even 32 nm linewidths, cost tens of millions of euros, making acquisition and amortization of the instrument impossible unless very high volumes are to be produced. For these reasons such instruments can only be owned by large IC-manufacturers. Because the cost of optical lithography grows rapidly as linewidths get smaller, research and utilization of alternative techniques are tempting. Although the driving force in the development of lithography has been electronics, there are many other applications that benefit from effective nanofabrication methods.

Perhaps the most interesting alternative lithographic methods for repetitive nanofabrication are interference and near field holographic lithography (Chapter 2.2), electron beam lithography (Chapter 2.3), and nanoimprint lithography (Chapter 2.4). All of these techniques were also utilized in this Thesis, although I worked only with NIL.

2.2 Interference Lithography

Interference lithography utilizes the interference of two or more coherent laser beams that form an interference pattern on the substrate. Using photoresists similar to those used in optical lithography, this interference pattern can be transferred to the photoresist and subsequently to the other layers on the substrate. Near-field holographic lithography is very similar to interference lithography. It uses a phase mask near the substrate to divide one beam into two diffracted beams propagating at different angles. These two beams interfere and generate a diffraction pattern. Both methods can produce patterns cost-effectively over large areas, but only

allow exposure of periodic patterns whose pitch is limited by the exposure wavelength. However, state-of-the-art exposure tools produce good resolution. With a high index immersion fluid system a 32 nm half-pitch has been demonstrated using an exposure wavelength of 193 nm (French *et al*. 2005) and a 12.5 nm half-pitch using an extreme ultraviolet light source at 14.5 nm (Solak *et al*. 2007).

2.3 Electron Beam Lithography

Electron beam lithography (EBL) is based on a beam of electrons focused on a small spot with a Gaussian shape, or on a beam of electrons cut down to the correct size and shape with an aperture. This beam is displaced with a magnetic field that is controlled with a computer. The beam exposes the electron beam sensitive material deposited onto the substrate in a similar fashion as a photoresist is exposed in optical lithography. EBL allows replication of geometrical data structures from the computer memory to the substrate. Therefore, it is used to generate templates for other lithographic techniques.

EBL systems offer high resolution, since the wavelength of the electron is very small (Vieu *et al.* 2000). The resolution of EBL is mainly limited by electron-solid interaction (forward and backward scattering of electrons and secondary electrons), which broaden the beam in the resist. A second major limitation for the resolution is the resolution of the resist (McCord and Rooks, 1997). For narrow patterns development of the resist is challenging, since intermolecular forces prevent dissolution of the polymer in the solvent, and the mechanical stability of the polymer is too low for wet processing (Vieu *et al.* 2000). There is also a practical limitation associated with throughput. As the beam is focused into a tiny spot it can deliver only a small current, and therefore the exposure time is increased. Moreover, high-resolution resist tends to require higher exposure intensity than low resolution resists (McCord and Rooks, 1997). At the same time, writing of large areas is very time consuming if the density of the patterns is high or the pattern geometry is challenging.

The registration of patterns in EBL is not necessarily nearly as good as the resolution of the system, because the substrate has to be moved over large distances during exposure. This

requires a fast and extremely accurate mechanical stage. High-end systems having a 10 nm registration accuracy and reasonable write speed can cost millions of euros. Even in high-end systems, writing a single wafer takes a long time. As a consequence, the exposure cost per wafer is substantial.

Electron beam lithographic systems based on the use of multiple beams are being developed at present to tackle the throughput problem. These kinds of systems are currently targeting the prototyping or small volume manufacturing of IC circuitry. The first "demo" systems are being sold to customers. In 2008, for example, Mapper Lithography delivered the first systems having 13,000 beams to CEA-Leti and the Taiwan Semiconductor Manufacturing Company to be explored in 22 nm manufactures (Mapper 2009; Wieland *et al*. 2009). The KLA-Tencor Corporation and the Defence Advanced Research Projects Agency (DARPA) have launched a cost-shared program to develop high throughput EBL systems containing a million beams. The system is targeted to the production of an astonishing five to seven densely patterned 300 mm wafers and up to forty sparsely patterned wafers per hour. The system is intended for the 45 nm node with extendibility to the 32 nm node and beyond (Petric *et al*. 2009). Although these systems produce a unprecedented direct writing throughput it is expected that it will take a long time before these systems migrate into mainstream lithography, due to their development status, complexity and cost of the instruments.

2.4 Nanoimprint lithography

Nanoimprint lithography (NIL) was introduced at 1995 by Stephen Chou (Chou *et al*. 1995). He demonstrated results from an experiment where a lab press was used to press together a patterned stamp, made from a SiO_2 coated Si-wafer, with a silicon substrate coated with a thermoplastic polymer poly(methyl methacrylate), more commonly called PMMA. Pillars having 25 nm diameters were successfully transferred from the template to the substrate. The process flow from the early paper is illustrated in Figure 1. One can argue that Chou's method does not differ much from earlier imprint methods; i.e., those that were used to make compact disks (*i.e.* Komatsubara *et al.* 1984), but the combination of a nanoscopic lateral scale and a thin residual layer allowing a subsequent pattern transfer to the underlying layers differentiates

Chou's work from others and defines NIL. However, nowadays the terminology related to different approaches of NIL is quite versatile and almost every nanoscopic molding process is called NIL.

The NIL process is a mechanical replication process. Surface reliefs from the template are embossed into a thin layer on the substrate. In principle, there are two basic versions of NIL. One is based on thermal embossing of thermoplastic polymers, while the other is based on UV-curable polymers. Some special imprint chemistries require both temperature and UV-light (Schuster *et al*. 2009), but they are not very common. The NIL process and imprint instrument are conceptually very simple, but allow extremely good resolution and a relatively fast replication process. Compared to optical lithography NIL does not require extreme ultraviolet light sources and special optics, which would increase the cost dramatically. In principle, NIL has no limitation in pattern geometry. Therefore, NIL can copy any pattern produced with EBL or by other techniques. In practice, if patterns have a high aspect-ratio or large distribution in pattern density or size, they can be very difficult to imprint simultaneously, as discussed later.

Thermal-NIL, as illustrated in Figure 1, was the original version. It uses a thermoplastic polymer spin-coated on the substrate. The thermoplastic polymer is heated above the glass transition point of the polymer, and the heated template is brought into contact with the polymer. Once the polymer has filled all the cavities of the template, the substrate and the template are cooled down and the template is separated from the substrate. A negative replica of the template is created on the polymer. In order to use the imprinted polymer for the pattern transfer to other layers on the substrate, the polymer left on the indented areas has to be removed. This residual layer (see Figure 1) originates from the fact that the flow of polymers is not free of resistance.

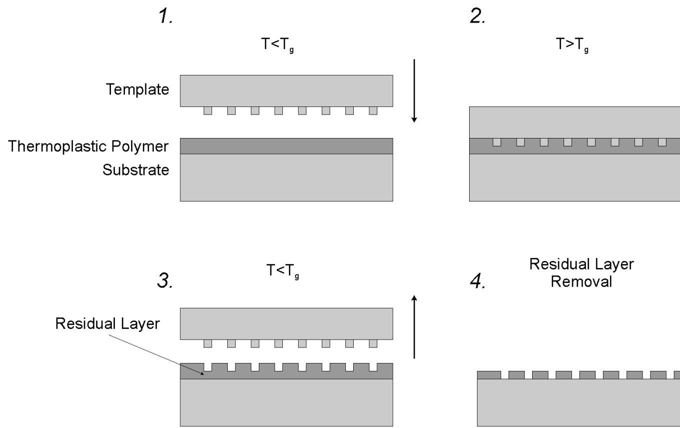

Figure 1. Thermal NIL-process. T_g refers to the thermoplastic polymer glass transition temperature.

Stefan's equation (Bird *et al*. 1977), describing the force needed to press two circular discs separated by a Newtonian fluid closer to each other suggests that the imprint force is inversely proportional to the third power of the residual layer thickness. The equation states that

$$F = -\frac{3\pi R^4}{h^3}\frac{dh}{dt}\eta_0. \tag{1}$$

In Eq (1) F is the applied force, R is the disc radius, $2h$ is the separation between the discs, and η_0 is the viscosity of the fluid. Stefan's equation implies that the displacement of fluid over large distances *via* thin channels requires a large force, or a small displacement rate. In particular, as the residual layer becomes very thin, resistance grows rapidly, and it is no longer possible to displace all material within a finite time.

The assumption that the fluid is Newtonian requires that it maintains its viscosity at constant temperature. This assumption is often valid. However, under high pressure and shear force molecular chains of polymers may stretch and therefore alter the viscosity of the fluid. Nonlinearity of the viscosity is described, for example, in references (Hoffmann 2002) and (Schift and Hayderman 2002). In addition to pressing two discs together it is important to understand the filling of small cavities with fluid to improve the model of the operation of NIL. A detailed descriptionof the filling of a cavity is given by (Rowland *et al*. 2005). They identify three

operating regimes for filling of a cavity depending firstly on the dimensionless ratio between the width (= 2*w*) and the height of the cavity (= h_c) to be filled, and secondly the ratio between the width of the indention in the template (= 2*s*) and the thickness of the residual layer (h_r) below the indenter determining the supply of polymer. These parameters are illustrated in Figure 2. For these regimes it is possible to analytically calculate the filling time of the cavity and to simplify the Navier–Stokes equations describing the generalized case.

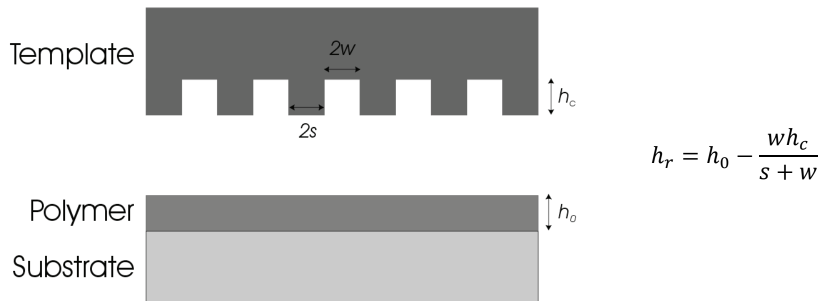

$$h_r = h_0 - \frac{wh_c}{s + w}$$

Figure 2. Definitions for symbols by (Rowland *et al.* 2005). The thickness of the residual layer h_r is calculated by assuming complete filling of the cavity, conservation of polymer volume, and neglecting large scale flow.

The case of a high aspect-ratio of the cavity ($w < h_c$) is described by pipe flow conditions where the flow resembles steady laminar fluid flow within a pipe. Under these conditions the flow is mostly vertical. For a low aspect-ratio of the cavity ($w > h_c$) the flow is mostly horizontal and can be governed by either viscous flow or shear flow, depending on supply of the polymer. For the case when $w > h_c$ and $s < h_r$ the operation mode is the Stokes flow (or creep flow) regime, where the viscous flow of the fluid governs filling. These conditions are met when the residual layer is thick. For the same case, with a thin residual layer ($w > h_c$ and $s > h_r$), the flow is governed by shear flow, the flow induced by short range deformation of polymer that induces a force gradient. The observations we made on stamp deformation in reference (P3) fit quite well to this model. Operation in the shear flow regime with a soft stamp causes stamp deformation while operating in the viscous regime eliminates it, even with a very soft stamp.

In addition to squeezing flow, also capillary force influencesthe flow of the polymer. In fact the whole replication process can be driven by capillary forces (Rowland *et al.* 2005) if the viscosity

of the resist is low, its surface tension high, and the amount of squeezing flow small (*i.e.* because of low imprint force). This is the case when the imprint pressure is small, for example. High solvent content of an imprint polymer promotes effective wetting of surfaces. Capillary force may also cause defects in imprints. Lazzarino *et al.* (2004) have shown that if the template and the polymer are not in complete contact this may induce wetting defects. These defects appear in areas where mold and polymer are in close proximity but not in contact.

A third consideration for NIL processes is the inclusion of gas. Imprinting traps gas in all cavities of the template unless imprinting is carried out in vacuum. Any trapping of air in the imprint pattern must be eliminated in order to achieve a perfect replication process. The simple solution of using a vacuum environment is somewhat challenging for design of the NIL tool, since it inherently reduces the throughput of the system and creates extra complexity. Additionally, a vacuum can easily modify the properties of the imprint polymer *i.e.* by reducing its solvent composition or enhancing evaporation. Most NIL tools reduce air trapping by applying nonparallel contact between the template and the wafer. For example, in the EVG tool used in this thesis the template and the wafer are slightly nonparallel. Therefore, when the template and the wafer contact, air is more easily squeezed out from between them.

To keep the amount of trapped gas small, flat molds with narrow low aspect ratio patterns are preferred. The excess gas can also dissolve into the resist. Solubility of gas may also be enhanced by using a thick resist layer. Then the concentration of gas is low, since the volume of the polymer is large. In addition, within a thick layer gas dissolves more effectively. A long imprint cycle promotes defect free imprinting because it promotes dissolution. High imprint pressure results in a faster dissolution of gas (Liang *et al.* 2007). Additionally, one may reduce the amount of gas by using properly tuned material systems and imprinting in various gas environments. For example, helium can be used since it diffuses more rapidly due its small size (Kim *et al.* 2006).

The NIL-process using UV-curable polymers is called UV-NIL. In this process, a layer of UV-curable fluid is spin-coated on the substrate, the transparent template is brought into contact with the fluid, and then cured using UV-light. The UV-curable layer must be exposed and cured through the template unless the substrate itself allows transmission of UV-light. The UV-NIL process has some inherent advantages over thermal-NIL:

i) UV-NIL is a room temperature process; therefore, time-consuming heating and cooling cycles are not needed.

ii) Room temperature processes eliminate the registration problems which originate from the different coefficients of thermal expansion (CTE) of the substrate and the template.

iii) Fluids having very low viscosity, from 2 mPa·s to 50 mPa·s can be used so that UV-NIL requires lower imprint pressures and shorter imprint cycles than thermal-NIL.

In addition to classifying NIL processes by their curing properties, the processes can also be classified by their strategy to cover large areas. In principle, NIL can be applied to the whole substrate by using a template that is as large as the substrate. However, one small stamp can be used repeatedly to cover large areas. These approaches are called “full field NIL” and “step and repeat NIL”. Both methods have their advantages and disadvantages, as summarized in Table 1.

In the case of UV-NIL, different processes can also be differentiated by the dispensing mechanism of the UV-curable polymer. The polymer can be dispensed as a uniform thin layer on the substrate by spin-coating. Alternatively, it can be dispensed as droplets(2) on pre-defined locations on the substrate by ink-jet or other means. Both methods have their advantages. Spin-coating does not require any special equipment, and can deposit highly uniform layers with minimal investment. Droplet dispensing allows polymer to be delivered directly to the location where it is needed by adjustment of the droplet density, as illustrated in Figure 3. Therefore the polymer does not need to flow over large distances, and throughput is improved in some cases.

(2) Droplet dispensing is also known as step and flash imprint lithography (S-FIL) or jet and flash imprint lithography (J-FIL).

Table 1. Comparison between "Full Field" NIL and "Step and Repeat" NIL.

Attribute	*Full field NIL*	*Step and Repeat NIL*
Instrument complexity and cost	Very low to medium	Medium to very high
Throughput	Higher, since larger area is imprinted	Lower, since large area has to stitched from small areas
Requirement for planarity of the template and the substrate	Higher	Lower
Cost of the Template	Very high. Depends on substrate size	Medium. Depends on imprint field size
Die size	Not limited	Limited by individual imprint field
Within field pattern registration	Lower, due to larger area	Higher, due to smaller area
Over the substrate pattern registration	High, template dependent	Low to very high depending on instrument quality
Alignment accuracy	Medium	Medium to very high in advanced systems
Overlay accuracy	Lower, limited by the pattern registration over large field or alignment	Higher since pattern must be aligned and registered over smaller field

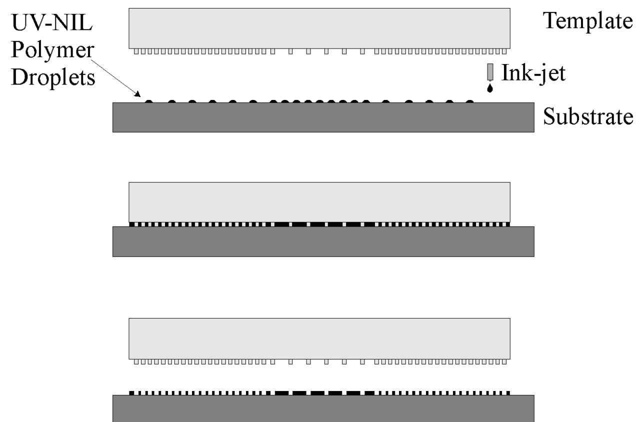

Figure 3. Sequence for droplet dispense NIL. Step 1: Deposition of the UV-curable polymer using ink-jet or similar instrumentation. The density of the droplets can be chosen based on the template pattern volume. Step 2: Imprint and UV-cure. Step 3: Separation of the template.

Droplet dispensing also helps when imprinting layers containing local variations in nanopattern density, and consumes significantly less material than spin-coating[(3)]. Droplets of strongly hydrophobic materials can be deposited onto the substrate, whereas spin-coating of these materials is difficult. Although this dispensing method is in many ways advantageous, it requires special instrumentation capable of first delivering potentially vast numbers of droplets with accurate volumes (from pico-litres to micro-litres depending on the droplet density) to the correct positions on the substrate, and then aligning the template correctly to the droplet pattern.

2.5 State-of-the-art in NIL

The first published NIL paper already demonstrated a 25-nm pattern diameter and pattern transfer using the lift-off technique (Chou *et al*. 1995). Later, a 10-nm pattern diameter was demonstrated by improving the resolution of the template (Chou *et al*. 1997). Both these records were based on the use of EBL-written templates that limited the resolution. The same group demonstrated a 6-nm linewidth using a template made out of an epitaxially-grown GaAs/AlGaAs superlattice (Austin *et al. 2005)* As early as 2004, Hua had demonstrated the smallest linewidths, as low as 2 nm, using a carbon nanotube-based template (Hua *et al*. 2004). This demonstration was considered a resolution record for imprint lithography. However, Hua's patterns were not transferred to the underlying substrate.

Early imprint experiments were able to pattern areas of a few cm^2 (Chou *et al*. 1997), and some demonstrations, like (Austin *et al*. 2005), were made on tiny areas of just some µm^2. However, in order to unleash the full potential of NIL larger imprint areas were required. Once the potential of NIL was acknowledged, imprint experiments were made on 100 mm, 150 mm and 200 mm wafers (Ross *et al*. 2003, Li *et al.* 2003, Perret *et al.* 2004). Now the largest imprint areas cover 300 mm wafers using imprinting with a soft stamp and air cushion press (Chang *et al.* 2005) and 300 mm x 400 mm substrates using a soft roll-shaped stamp (Cho *et al.* 2009). With roll-to-roll imprinting very large areas can be covered in one imprint batch. For example, the DVD manufacturing system by (Oha *et al.* 2007) demonstrates imprinting of a very long, 0.15 m by 1400 m, sheet.

[(3)] A uniform 100 nm layer requires just 10 nl / cm^2 of polymer.

A state-of-the-art step and repeat system from Molecular Imprints Imprio 300 has demonstrated a throughput of 4 wafers per hour for 300-mm wafers using an imprint field of 26 mm × 32 mm. Although the current throughput record for the step-and-repeat system is rather modest compared to optical lithography systems, the company believes that the throughput can be further improved by clustering these low-cost imprint heads together, and by improving their process. In this way it would be possible to realise a high throughput at lower cost than competing optical lithography systems (Sreenivasan *et al*. 2009).

The alignment accuracy record for NIL is also set by the Molecular Imprints Imprio 300 system. The system has demonstrated a 3σ [(4)] alignment accuracy of 16 nm using thick glass templates which had Moiré-alignment marks. The instrument could deform templates *in situ* by some nanometres in order to fine-adjust the overlay of the template to the substrate. They also utilized a feed-forward strategy that allowed correction of the overlay based on the measurements of the previous overlays (Sreenivasan *et al*. 2009).

Modern NIL systems targeted for high brightness LED manufacturing reach 60 wph throughput for 3″ wafers (Miller *et al.* 2008) and systems designed for imprinting large 200 mm substrates reach throughput of 30 wph (Obducat 2010). The best reported throughput values for NIL systems are reported by Molecular Imprints Inc. For full field UV-NIL systems they demonstrated throughputs as high as 180 wafers per hour using their HD2200 system designed for a hard disk pilot production (Brooks *et al*. 2009). Dual layer Blu-ray discs, used in optical storage, are replicated one disc per second using a thermal embossing system. In this application nanoimprinting is used to make the topmost layer on the injection molded substrate (Ohta *et al.* 2007). Even higher throughput values have been demonstrated using so-called roll-to-roll imprint systems. Here, a substrate consists of a roll of plastic or polymer film. The film is fed from a spool between a heated imprint drum and a roller. The stamp is attached around the imprint drum. Single layer DVDs are produced at a rate of 8 disks per second by roll-to-roll imprinter and Ni-stamp hot embossing (Ohta *et al.* 2007). It should be noted that the fabrication of DVDs and blu-ray discs does not require pattern transfer with etching; therefore very thick residual layers can be used, which improves the throughput.

[(4)] 3σ: More than 99 % of randomly distributed measurement points fall within specified boundary

For further information about various aspects of NIL, readers are encouraged to read the excellent reviews written by Costner *et al.* (2009), Schift (2008), Guo (2007), Guo (2004) and Sotomayor Torres (2003).

3 Soft stamp UV-nanoimprint lithography

Soft stamp UV-NIL is one of the most interesting nanoimprint methods, due its outstanding cost effectiveness. As the name implies, this method utilizes soft and sometimes flexible working stamps, replicated from the template. The softness of the stamp makes the imprint process more robust and economical. When the stamp is soft it can deform locally, for example, when a particle is trapped between the stamp and the target wafer. This improves the yield of the process, since with a soft stamp a small particle destroys only a small part of the imprint area. Stamp softness also allows for imprinting of a large area in a single step, while maintaining a uniform residual layer. High uniformity is possible because a soft and flexible stamp conforms to the overall non-flatness of the substrate. On the other hand, fully rigid hard stamps can typically be used to imprint a maximum of one square-inch area, in a single step. This is because any potential unevenness of the substrate surface, within the imprint area, adds to the nonuniformity of the residual layer. This is important to realize, since it is not always possible to use sufficiently flat substrates. In particular, when the linewidth is narrow and the pattern's height is small, the residual layer must be highly uniform. The problem associated with hard stamps is illustrated in Figure 4.

One of the best features of soft UV-NIL is that it can be applied using modern UV-mask aligners equipped with special tooling. The mask aligner is, in any case, the workhorse of microlithography processing, since it is often the best tool for patterning microscopic features. The increased cost of the mask aligner, due to NIL-tooling, is insignificant compared to any other feasible nanolithography solution. A manual mask aligner, equipped with NIL tooling, can produce from ten to twenty wafers per hour, and automated systems reach even higher throughputs. At the moment NIL tooling is available for EV Group, Suss Microtech and OAI-mask aligners. These tools typically allow a submicron alignment accuracy and can be operated in manual, semi-automatic, or fully automatic modes.

Conformal imprinting, on nonflat substrates, is also possible to achieve with hard stamps since, in principle, all stamps are flexible under high enough pressure. This has been demonstrated, for example, in reference (Perret *et al.* 2004), where a 200 mm wafer is patterned using a 200 mm silicon wafer as a stamp. Here, pressure as high as 8 bar was used to achieve full contact. When only a tenth of the pressure is available, as is the case in mask aligners, a more flexible or soft stamp is required. For example, reference (Plachetka *et al.* 2004) demonstrates imprinting of a 100 mm wafer using a mask aligner and a soft stamp under a low imprint pressure of 0.5 bar. As discussed earlier, stamp deformation allows large area contact but at the same time causes undesirable effects. Undesirable deformation may be caused by nonuniform pressure distribution, arising from *e.g.*, pattern density variation (Gourgon *et al.* 2005) or a large pattern (P3). Lazzarino *et al.* (2004) discuss mold deformation as a function of the pattern density and underline the importance of layout design. They concentrate on use of hard stamps and demonstrate how a long imprint cycle (60 min) under high pressure (50 bar) helps to reduce the deformation. Bender *et al.* (2004) have discussed the use of soft stamps and the importance of pattern geometry and imprint pressure to achieve uniform pattern transfer.

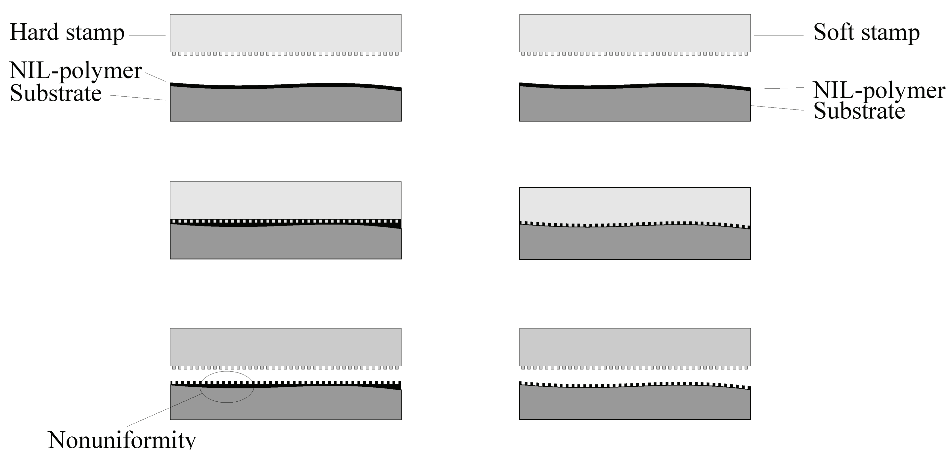

Figure 4. Comparison between soft and hard stamp technologies. Left panel: Process flow for a hard stamp. It shows how non-uniformity of the wafer is transferred directly to the residual layer, since both the stamp and the substrate are rigid. Right panel: Process flow for a soft stamp. This stamp can conform to the waviness of the wafer, thus improving the uniformity of the residual layer.

Some systems (*i.e.* step-and-repeat systems from Molecular Imprints Inc.) operate at low imprint pressure using hard stamps which do not deform under such process conditions. This is made possible by keeping the imprint area small enough for the the imprint site to be sufficiently flat to produce the desired residual layer uniformity. Another possibility is to first use a blank imprint stamp to planarize the substrate. A subsequent imprint step is then made on the planarized layer. With appropriately selected materials and etch processes, pattern transfer can be improved (Sun *et al.* 1998). The advantage of non-deforming imprint stamps is the elimination of the unwanted stamp deformation. However, it comes at the expense of the imprint area which can be covered by a single imprint.

As deformation is necessary for large area imprints but harmful for replication accuracy, it is important to engineer stamps that have proper flexibility. References (Bietsch and Michel, 2000) and (McClelland *et al*. 2005) discuss the compliancy of stamps and show how suitable imprint pressures as a function of wafer unevenness or roughness and its lateral size can be determined. Magnification (lateral stretching) of the imprint field under pressure was studied by (Lan *et al.* 2009). They concluded that deformation error in the registration is from 10 to 56 μm over a 4 cm^2 imprint field. In the calculation they used a pressure of 0.25 bar and varied the thickness of the soft stamp from 0.5 mm to 2 mm. This huge error has to be considered when designing and fabricating soft stamps.

3.1 Fabrication of large-area templates

Based on experience, the most severe limitation for the potential of NIL, especially for NIL using full wafer sized stamps, is the cost of the mastering. When patterns are narrow and dense the exposure rate of any direct write system is slow. Therefore, the templates can be very expensive or non-feasible to fabricate. At the moment, the only generic method to circumvent this problem, and to make large-area stamps, is the use of step and repeat lithography (optical or NIL), since it allows replication of small dies to large area dies. The benefit of optical lithography is that it uses reduction lenses that scale down the dimensions of the photomask. For this reason, the original template (the photomask) can be fabricated with looser tolerances for particle size, linewidth and registration of the patterns than a final large-area NIL template. Step and repeat NIL allows narrower linewidths than optical lithography, and the NIL steppers are more accessible than

state-of-the-art optical lithographic tools. Both lithographic options are available from commercial vendors to prepare large-area templates.

We have studied the use of NIL templates fabricated from quartz mask blanks, Si-wafers, silicon-on-insulator (SOI) wafers, and Si wafers with or without PECVD (plasma enhanced chemical vapour deposition) -deposited SiO_2 top layers. All of these material systems have a common SiO_2 surface chemistry (thin surface oxide or bulk oxide) and similar adhesion properties. The main considerations for template fabrication are: etch depth uniformity, surface quality and flatness, etch profile and templates ruggedness. In many applications the quality of the EBL tool and processing must be excellent in order to overcome restrictions that device physics imposes.

When the linewidth of the patterns or the density of the patterns change over the template, etch depth uniformity issues may arise. These phenomena are referred to as reactive ion etching-lag and aspect-ratio [(5)] dependant etching. Dense and narrow features tend to etch more slowly than isolated and wide features. Both of the material systems, SiO_2-coated Si wafers and SOI-wafers, allow improved control of the etch depth by utilizing an etch-rate difference between Si and SiO_2. PECVD allows easy control of the etch depth but has higher surface roughness compared to SOI-wafers, which have to be bought from the wafer manufacturer with correct silicon layer thickness. On the other hand, SOI-wafers are almost atomically smooth. They provide the best platform for fabricating large-area templates in terms of quality. The main inspection method for template cleanliness and quality is the scanning electron microscopy. Electrically conducting silicon templates are therefore preferred. However, a quartz template offers the lowest CTE from these materials and provides a most stable pattern registration.

Pattern depth and sidewall profiles influence the adhesion between the template and the imprint resist. Obviously, shallow and smooth structures require less force since their surface areas are smaller. A positive etch profile (sidewall angle $< 90°$) promotes a lower adhesion force to NIL-resist than a straight sidewall angle, but it is easier to maintain a correct linewidth by means of the 90° sidewall angle. Negative etch profiles (sidewall angle $> 90°$) have high adhesion forces and usually cannot be replicated, although such profiles would be ideal for lift-off processing.

[(5)] Ratio between height and width of the pattern

However, replication of a slanted grating facing in opposite directions has been demonstrated, showing that even negative profiles can be replicated using certain material systems (Levola and Laakkonen 2007).

3.1.1 *Large-area templates using special methods*

There are several examples which prove that NIL templates can be made using special processes. These processes combine etching and deposition steps. Those steps can be controlled on the nanometre scale in a way that creates new nano-scale patterns having a specific shape. Alternatively, the templates may be based on bottom-up nanofabrication or certain phenomena occurring in nature. The application range for templates fabricated using these methods is always limited, because the information content of the patterns is very low, and the patterns allow little design freedom. However, sometimes these techniques are useful. Table 2 summarizes some of the demonstrated methods.

Table 2. Some examples from special methods used to make templates for NIL.

Feature	Fabrication method	Reference
Closed loop structures	Deposition of a conformal layer on the sidewall of a pillar and removing the vertical pillar	(P1)
Frequency doubling of a grating	Angled evaporation to a pre-fabricated grating. 30 nm pitch from 60 nm pitch.	Yu *et al*. 2006
A loosely ordered hexagonal array of pillars.	Aluminium stamp fabricated from a porous alumina surface. Melting a sputtered Al-film on top of a porous alumina substrate. Removing alumina and using aluminium as a stamp	Lee *et al*. 2005
"Moth eye" antireflection surface	Using a wing of an Australian greengrocer cicada "cyclochila australasie" (an insect) as a template	Kostovski *et al*. 2008

3.2 *Soft stamps*

Since the template is often expensive it is common practice to prepare a working stamp from the template. Such a replicated stamp can be used to make several imprints, therefore minimizing

the risk of damage to the original template. The stamps may also have different physical properties than those of the template. For example, an SOI-wafer is in many ways an ideal substrate for the template, as described earlier. However, it is opaque and, thus, unsuitable for UV-NIL. The replicated stamp might also have advantageous mechanical properties, such as a soft surface and flexibility. The softness of the stamp may be tuned by the material selection (Schmid and Michel 2000) and by the geometry of the stamp, as illustrated by us in reference P3. A working stamp might have advantageous chemical properties, for example, stamps made of polydimethylsiloxane (PDMS) have very hydrophobic surfaces and do not require anti-adhesion treatment. Moreover, PDMS can absorb small amounts of solvent, which allows for improved wetting of the stamp surface.

Perhaps the simplest soft stamp is a thick PDMS slab, typically made from commercially available PDMS brand Sylgard 184, also known as soft-PDMS or s-PDMS (Dow Corning Inc., USA). The stamp is cast in a chamber, using the template and anti-adhesion treated glass (see the stamp in Figure 5a). This stamp can be used to replicate nanopatterns, but it does not offer high accuracy because PDMS has a high CTE, and the stamp does not have a supporting structure which would prevent the soft material from deforming laterally. More advanced geometries of the soft stamp are presented in Figure 5b and Figure 5c. In Figure 5b the s-PDMS slab is bonded to glass. This improves the accuracy of the stamp, because various glasses have significantly lower CTEs (from 0.5 to 8 ppm/°C) and higher elastic modulus than those of soft materials. For these reasons glass reduces lateral deformation, which may arise from thermal expansion mismatch between the stamp and the substrate or from other factors during imprint. Figure 5c improves the stamp concept of Figure 5b; since the nanopatterned layer of the stamp is composed of a different material than that of the soft compliant layer. Such a composite structure has the advantage that the pattern layer can be made of a harder material, such as hard-PDMS.

The stamp in Figure 5d further improves this concept by introducing a thin layer of glass between the hard polymer and the layer of s-PDMS. In this geometry, the thickness of the patterned polymer can be tuned nearly at will, and is backed by a thin glass plate (for example 50 μm thick). Since a glass layer is bonded close to the nanostructures, effectively anchoring the patterns, lateral deformation of the pattern is minimized. The advantage of the thin glass in this geometry comes from the fact that the bending stiffness and the stretching stiffness scale to the

third and the first power of the thickness of the sheet, respectively (McClelland *et al*. 2005). Therefore, a thin sheet is very compliant but simultaneously maintains its lateral dimensions. In addition, bending deformation of the glass sheet is proportional to the fourth power of the lateral scale (McClelland *et al*. 2005). Therefore the glass sheet deforms only very slightly on the scale of the patterns. In this stamp concept sort range deformation is caused by a thin patterned layer. With this kind of stamp concept we have demonstrated registration reproducibility better than 8 ppm (80 nm/cm) from imprint-to-imprint over a 3-inch substrate and shown that local lateral deformations are almost non-existent (P4).

We expect that three factors limited the imprint accuracy to this level; the most significant effect was the temperature variance of the cleanroom, which caused thermal expansion problems since glass and the substrate have different CTEs. Other error sources were in the overlay measurement accuracy when studied by optical microscope, and variations in imprint pressure. The backing glass plate in Figure 5d is optional. When this plate is employed it eases stamp handling with NIL tools, but without this plate the stamp is fully flexible and is easily peeled from the substrate after imprint.

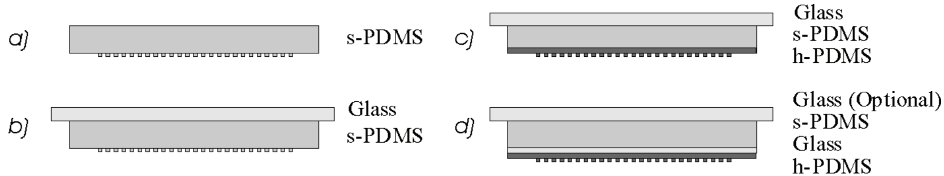

Figure 5. Different stamp schemes. a) Thick PDMS slab. b) PDMS slab backed with glass. c) Composite stamp containing a hard PDMS pattern layer. d) Stamp having thin intermediate glass for improved stability.

Table 3 summarizes materials used in soft stamps. It should be noted that the mechanical properties of these materials may be altered to some degree by processing conditions and mixing ratios.

We have applied silicones Sylgard 184 (also known as s-PDMS, Dow Corning Inc., USA) and Optical Encapsulat 43 (Gelest Inc., USA) as compliant, non-patterned cushion layers since they are relatively soft and durable. They can be spin-coated onto a substrate. It is also possible to cast them into a mold. Spin-coating offers good coating uniformity (> 98 %), but only about 30-μm

layers can be coated in a single spin-coat cycle. Thicker layers require multiple spin and cure cycles. Casting of thick uniform layers is problematic even with an almost perfectly flat mould. When we cast 2 mm thick slabs using these soft materials we observed pits and hills of several tens of microns in height. The lateral size of these features was in the sub-10 mm range. We believe that they were caused by small non-uniformity in volumetric shrinkage during curing. In particular, pits in the compliant layer should be avoided because they will lead to the creation of areas that are not in contact during imprint. Our observations concerning the uniformity of the compliant layer are in good agreement with the reported values of Glinsner *et al*. (2007).

Sylgard 184 is widely used as a patterned layer in the stamp. We also tested this approach. Due to the excessive softness of Sylgard 184 we often observed deformation of nanopatterns during the imprint cycle, and pairing of neighbouring patterns during stamp manufacturing. We believe that the neighbouring patterns stick together (pair), as illustrated in Figure 6, because friction during the separation step generates surface charges. The generated electric field is several hundreds of volts/meter at one centimetre distance from the stamp, measured with a field mill-based static electric field meter. On the nanoscopic scale the field is non-uniform and causes forces strong enough to bend the patterns together. Interestingly, as the patterns move, the electric field changes and the neighbouring patterns can, under the right circumstances, change their pair. This can be observed through the optical microscope as a dynamically and chaotically changing pairing. Unfortunately, as the surface charge discharges over time, the patterns do not return to the non-paired situation. This is because the PDMS surfaces kept in contact react chemically and become glued together. Pairing can be reduced by a reduction in aspect-ratio, by an increase in pattern spacing, or by using stiffer stamp materials; *e.g.,* h-PDMS and Ormostamp (introduced later). Long grating lines and tightly spaced pillars on PDMS are most prone to pairing with their neighbours. Larger patterns are less likely to pair than smaller ones, and the softness of the stamp causes less deformation with microstructures than with nanostructures. For this reason Sylgard 184 is a rather popular material for micro-structuring of UV-polymers, but on the nanoscale more rigid materials are required.

Table 3. Materials used in stamp fabrication. Based on references Fuard *et al*. 2008, Choi and Rogers 2003, Gelest 2009, Dow Corning 2009, Kim *et al*. 2004, Klukowska *et al*. 2009, Micro Resist Technology 2009a and 2009b.

	s-PDMS	**h-PDMS**	**Ormostamp**	**Optical Encapsulat 43**
Young's modulus	1.8 MPa	8.2 MPa	650 MPa	Not known
Elongation at break (%)	160	7	Low	75-100
Scrach hardness (MPa)	4.77	0.02	36	Not known
Durometer, Shore A	48	79	Not known	5-15
CTE (ppm/°C)	325	Not known, expected to be similar to s-PDMS	For similar materials 60-130	Similar to Sylgard 184
Curing	Temperature	Temperature	UV-Light	Temperature
Surface energy	26 mN/m	Similar to s-PDMS	High	Not relevant
Viscosity (mPa·s)	4575	Tunable	410-460	800-1500
Mixing	Two part (1:10)	Four part + solvent	Not needed	Two part (1:1)

So-called hard PDMS (h-PDMS) was developed at IBM in 2000 (Schmid and Michel, 2000). They tried to formulate a better imprint material by trying different combinations of vinyl and hydrosilane end-linked polymers and vinyl and hydrosilane co-polymers, with varying masses between cross-links and junction functionality. A nanoimprint resolution record of 2 nm (Hua *et al*. 2004) was demonstrated using soft h-PDMS stamp. Based on Schmid's work and studies by our group we started to use a formulation according to Table 4. Toluene was used to dilute h-PMDS because it has very low viscosity (0.590 mPa·s) and quite a suitable dipole moment. When toluene is mixed with the h-PDMS pre-polymer these properties improve h-PDMS's ability to fill all of the nanocavities of the template (Kang *et al*. 2006; Koo *et al*. 2007). The toluene content in the h-PDMS can also be used to tailor the thickness of the spin-coated h-PDMS, as proved in our publication (P3). A good thickness control reduces stamp deformation in certain stamp geometries, as will be discussed later.

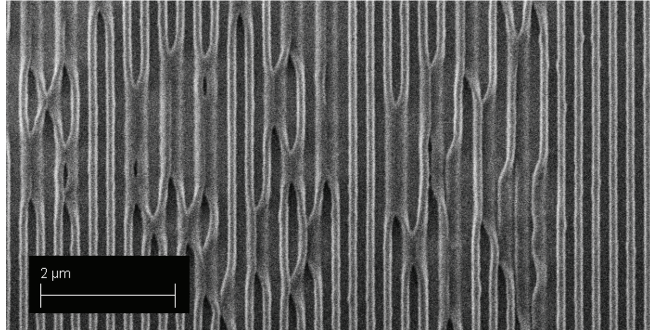

Figure 6. Scanning electron micrograph of a pairing effect on a soft stamp.

Table 4. The h-PDMS recipe used by our group.

Amount	Brand name	Substance	Role of the substance
3.4 g	VDT-731, ABCR GmbH	Vinylmethylsiloxane-Dimethylsiloxane	Prepolymer
0.75 g	HMS-501, ABCR GmbH	Methylhydrosilane-Dimethylsiloxane	Copolymer
10 mg	SIP6831.1, Gelest Inc.	Platinumdivinyltetramethyldisiloxane complex in xylene	Pt-catalyst
39 mg	LA16645	2,4,6,8 – Tetramethyl – 2,4,6, 8 – tetravinylcyclotetrasiloxane	Inhibitor
For example 40 m%	Toluene	Methylbenzene	Thinner

Ormostamp (Micro Resist Technology GmbH, Germany) is a recently developed UV-curable inorganic-organic stamp material. It is significantly harder than h-PDMS. Therefore, it must be backed with soft material in order to realize robust full wafer imprinting. Since it can be UV-cured, thermal expansion problems, observed when replicating thermally curable materials, are minimal. Using Ormostamp, change in lateral registration was only 14 ppm's across the wafer, measured from template-to-imprint. It is clear that in applications requiring the highest overlay accuracy the best approach is to use UV-curable stamp materials. Unfortunately, not many of these materials are commercially available.

We have mainly used Ormostamp as a replacement for h-PDMS, with a stamp geometry illustrated in Figure 5d. As h-PDMS is replaced by Ormostamp the stamp obtained is harder but as flexible. Unlike h-PDMS, Ormostamp requires anti-adhesion coating, but when coated properly with fluorosilane, Ormostamp shows better release properties than h-PDMS. In addition, Ormostamp is more chemically inert than PDMS. We have found that with PDMS many of the NIL resists do not cure properly. Therefore, the lifetime of the stamp might be short when used with these resists. It is often suggested that improper curing occurs simply because of oxygen out-diffusion from PDMS. We observed that some resists (*i.e.* mr-UVCur06 from Micro Resist Technology) worked better with Ormostamp than with h-PDMS.

Figure 7 and Figure 8 provide clear-cut evidence for the stability of silanated Ormostamp. These figures are from a series of wafers (25 pcs) that are patterned with properly anti-adhesion coated Ormostamp. The quality of the imprint remains constant across the whole batch. The batch was made at high throughput (~19 wph). The main process parameters influencing the throughput were: 10-s imprint time and 2-minute exposure time (7.5 mW/cm^2). Manual loading and unloading of the wafer took roughly one minute per wafer. It should be noted that our imprint system is not equipped for high throughput. It has a low-intensity light source which limits the cure time. In the same system, it is possible to achieve a larger throughput by using an order of magnitude higher exposure intensity. During the imprint series, wear of the fluorosilane coating reduced the contact angle of the stamp from 112° to 91.5°. This reduction indicates that the stamp should be re-coated.

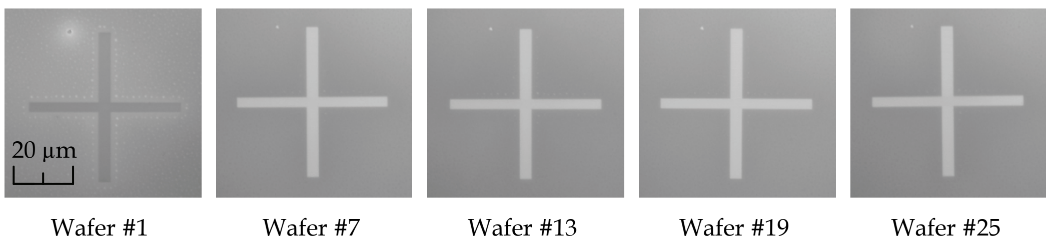

Figure 7. Microscope images taken from a series of 25 wafers imprinted using a stamp made of fluorosilane-coated Ormostamp. In Wafer #1 we used a layer stack different from the other wafers, which explains the slight difference in colour.

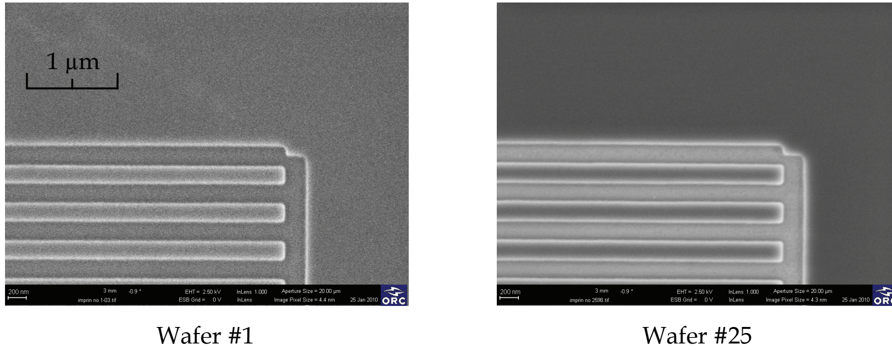

Figure 8. High resolution scanning electron microscope (SEM) close up from wafers #1 and #25 provides evidence that patterns show no reduction in quality after 25 successive imprints with the same stamp.

In many cases softness of the stamp is a trade-off between process robustness against wafer non-ideality, and vertical deformation due to an uneven load across the imprint field. A soft stamp improves the yield, since any possible particles only deform a small area of the imprint (see Figure 9, left panel). On the other hand, stamp softness complicates the process because it causes harmful bending under a locally varying load. This change in load is caused by the patterns in the stamp (see Figure 9, right panel). The deformation can be compensated for by increasing the thickness of the resist (P3), as the liquid resist layer effectively distributes the local pressure over a large area. We have observed that a low-viscosity NIL resist distributes pressure more efficiently than a high-viscosity resist. Although it is possible to imprint very high resolution imprints with this stamp (we have demonstrated 24-nm linewidth, P1), the softness of the stamp limits the resolution of the transferred patterns in some cases. Dense and small nanopatterns are relatively straightforward to imprint with a sub-10 nm residual layer, since the stamp load is uniform across the whole imprint field. However, if an imprint contains both wide and narrow patterns (as some of our samples do), isolated patterns, or if the density of patterns changes over the imprint field, vertical deformation of the pattern layer must be compensated for by a thick residual layer. When the thick residual layer is removed with plasma etching, the smallest patterns might be washed away, since the linewidth tends to be reduced during removal of the residual layer.

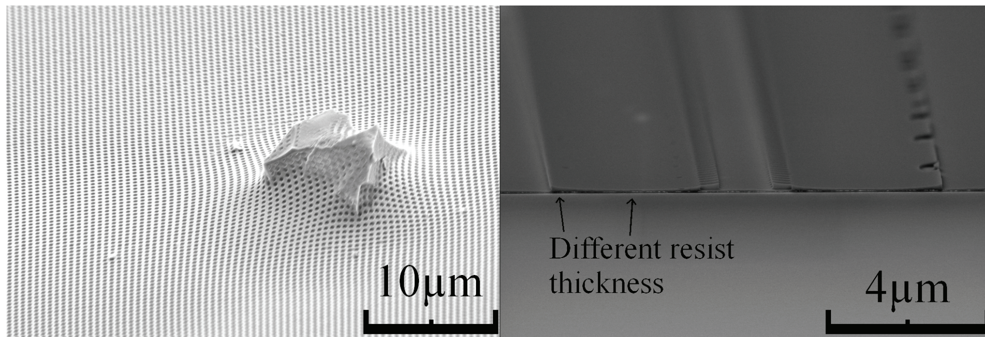

Figure 9. This figure illustrates advantages and disadvantages of soft stamps. Left panel: Softness has saved the imprint, since the pattern is only destroyed over a small area. Right panel: The imprint pattern is vertically deformed, since the relatively large pattern (~3 μm linewidth) does not have enough mechanical support.

The stamp concept in Figure 5d can significantly reduce the unwanted *vertical* deformation of the stamp, compared with other soft stamps, since the thickness of the pattern layer can be tuned (P3). The stamp with the thinner layer exhibits smaller vertical deformation on the microscopic scale. It is also effectively harder than the stamp with the thick layer, although both stamps are made of the same materials. It is worth noting that although hardness of the stamp can be tuned on the microscopic scale by tuning the h-PDMS layer thickness, on the wafer level the stamp is still fully soft since a thin layer of glass backed by a very thick elastic layer deforms easily across a wide (> 100 μm) lateral scale.

In addition to optimisation of the stamp geometry or material properties, vertical deformation can also be alleviated by a load sequence and a pattern layout. Obviously, low imprint pressure causes minimal deformation, but at the same time some force is required to overcome non-flatness of the substrate. It was demonstrated (P4) that by applying a dual sequence imprint process containing first a high pressure contact step and then a low pressure deformation release step, a better overall quality was attained when compared to the traditional single step process.

Many devices allow a reduction in deformation in the design phase. Isolated patterns, wide patterns, and patterns having density variations are the most difficult to imprint. Interestingly, the situation is similar, for example, in dry etching (Babin et al. 2005), chemical vapour

deposition (Cheong 2003), and chemical mechanical planarization (Park et al. 2001), which may suffer from similar layout restrictions. However, it is worth noting that many of the physical principles for uniformity reduction are somewhat similar across these processes; *i.e.*, limitations in mass transfer and pressure non-uniformity. For example in dry etching, etch rate uniformity can be reduced by a density variation in patterns because etching gas is consumed at the highest rate in the areas where the pattern density is the highest. Because of limited diffusion of the gas from a low pattern density area a difference in partial pressure of the etching gas is generated between these two areas. This difference causes lower etch depth in the high density area.

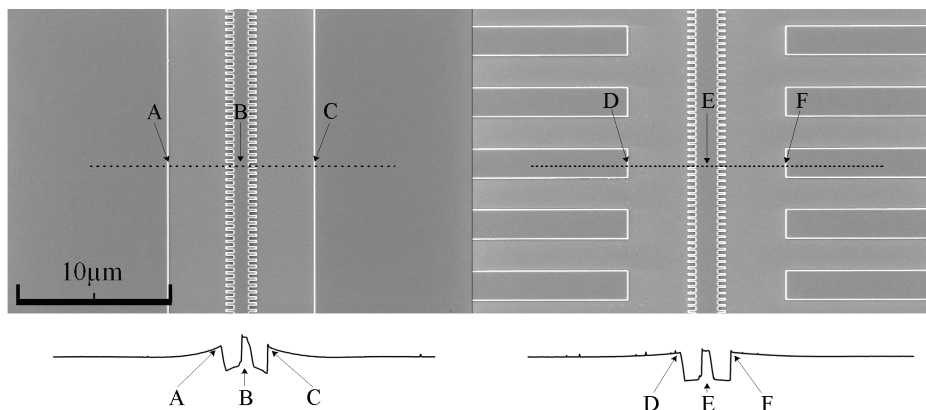

Figure 10. Unoptimized pattern layout (left) *versus* more optimal (right). Both layouts can act as identical waveguides for distributed feedback laser diodes (DFB-LDs) but the pattern layout on the right is designed to cause less vertical deformation. Deformation of the imprint is illustrated on the surface curves below the electron microscope images. The dashed line on the electron microscope image represents the place from which the surface graph has been obtained. The letters indicate distinguishable pattern shapes, making it easier to compare the graph with the image.

It is often possible to design the device layout in a way that circumvents these problems by, for example, placing dummy patterns which increase the pattern density without sacrificing the device functionality. We present in Figure 10 two different ways to realize a nanopatterned waveguide. The panel on the left (Figure 10) shows a straightforward way to realize the component. In this case the waveguide is isolated[6] and surrounded by an area having zero pattern density. The waveguide layout on the right corrects the problems of the non-uniform pattern density. It is surrounded by a grating having a 50% pattern density. Therefore,

---

[6] Spacing between parallel waveguides is 300 μm.

consumption of the resist and distribution of pressure are more uniform across the imprint field. As a result, the layout on the left exhibits as much as 3.4 times more vertical deformation compared to the layout on the right under identical imprint conditions. The drawings shown below the scanning electron microscope images give surface profiles of the imprint, obtained by an atomic force microscope.

3.3 Anti-adhesion treatment

Nearly all of the template materials require coatings which make it easier to separate the two surfaces. It is possible to use automated tools to deposit these coatings (i.e. from Applied MicroStructures Inc., USA) or to outsource the coating step (i.e. to DTI, Denmark). These methods are typically developed for SiO_2-covered surfaces. However, since we required coatings also on polymers in addition to very rapid turn-around times, we developed our own methods for coating the stamps.

There are three factors that need to be evaluated when applying the anti-adhesion layer. Obviously, factor one is to study how the anti-adhesion layer improves demoulding properties. Often this issue is addressed simply by measuring the contact angle of a wafer. The contact angle is proportional to the surface energy. A surface having a high contact angle and, therefore, being hydrophobic, is believed to be ideal for NIL. However, a more correct way is to evaluate the force needed to separate (fracture) the template from the resist or the stamp material. The contact angle and fracture strength do not necessarily correlate with each other because hydrophobic surfaces are not necessarily chemically inert (Houle *et al*. 2007). Secondly, coatings must be evaluated by their wear properties; *i.e.*, how many replicas can be made from the template before the anti-adhesion coating must be replaced. Finally, one must evaluate to what extent the coating distorts the dimensions of the pattern.

We used different anti-adhesion layers for different purposes. Amorphous fluoropolymer, Cytop (Asahi Glass Company, Japan) was one of the candidates. It has excellent transparency in the UV-region, a high contact angle (110° for water), high chemical resistivity, and it can be patterned with thermal embossing. These properties make it a highly attractive chemical for NIL. We applied diluted Cytop (0.18 m% of Cytop in solvent) by spin coating. The template was

dried with spining and the remaining solvent was driven off using a hot plate. Baking at 180 °C for one hour polymerized Cytop. This simple procedure allowed us to coat the template with 6 to 7 nm layer of Cytop.

Secondly, we tested a self-assembled monolayer (SAM) of fluorosilane as an anti-adhesion layer. One of these molecules was 1*H*,1*H*,2*H*,2*H*-perfluorodecyltrichlorosilane (CF_3–$(CF_2)_7$–$(CH_2)_2$–$SiCl_3$), better known as FDTS. This fluorosilane molecule silanizes the surface by forming chemical bonds between OH-ends of the surface and the $SiCl_3$-end of the silane molecule. It is believed that vapour phase deposition is preferred over liquid phase deposition since the later may induce wetting defects (Beck *et al*. 2002); we did not study this aspect but for this experiment we used vapour phase deposition. A detailed description of vapour phase deposition in a dry box is given by Zhou *et al*. (2008). Silanisation by a wet process is studied in detail by Hancer (2008).

It has been observed that excess humidity on the surface during deposition causes silane to polymerize in clusters (Britt and Hlady 1996). On the other hand, it is suggested that a thin layer of water would act as a lubricant layer for silanes (Brozoska *et al*. 1994). This interfacial H_2O layer allows migration of molecules on the surface so that the molecules can find positions where they best contribute to the formation of a complete, void free, monolayer. Some H_2O molecules are also needed to allow hydrolysis of Si-Cl bonds to Si-OH bonds (Brozoska *et al*. 1994). This water can be either on the surface of the substrate or be added to the silane. These OH-bonds of the molecule covalently bond with OH-ends of the surface or with OH-ends of silane. Gradually, condensation of a monolayer occurs. Illustration of the formation of SAM is shown in Figure 11.

When these two coatings are compared with each other, the advantage of FDTS coating is in its ability to maintain dimensions. Although the Cytop coating is very thin, it increases the linewidth somewhat and distorts the pattern‘s cross-sections by rounding them from the top and the bottom. However, it maintains the pattern‘s linewidth uniformity very well, as shown in Figure 12.

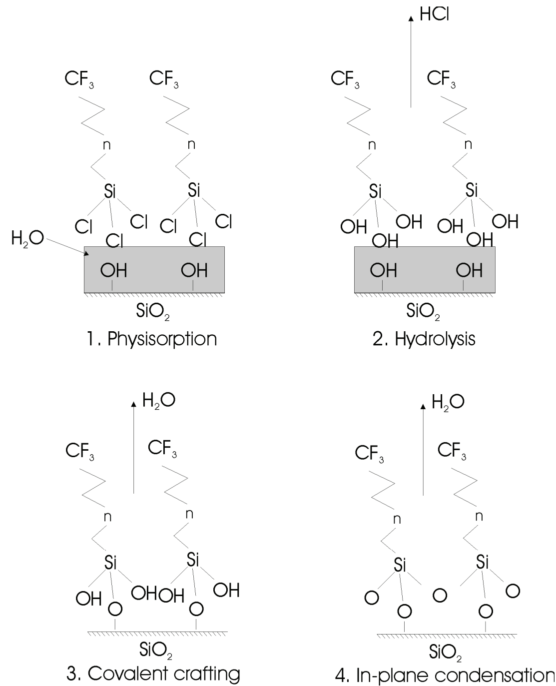

Figure 11. Formation of fluorosilanated SAM in four steps.

Actual release properties are illustrated in Figure 13. These properties describe the fracture strength needed to separate an anti-adhesion coated template from a small stamp (150 mm^2). In this experiment we used a 380-µm thick silicon wafer as a template and a 1-mm thick glass substrate as stamp backing glass. Ormostamp was used as the pattern layer. Both the template and the stamp are rigid. Therefore only one fracture occurs per separation, and the release can be quantified with a single number. Tests are made using a Dage 4000 (*Dage Holdings Limited, UK*) multi-purpose bond tester. The Dage tool is usually used to study the strength of wire bonds or solder joints, but we modified the geometry of the instrument in order to use it to test the adhesion properties of the stamp/substrate or the template/stamp interface. We prepared a vacuum chuck which made it possible to mount the template and used the shear test tool to push the stamp at a constant velocity until the software recognized that the stamp and the substrate were separated. The bond tester software plotted the applied force as a function of time and reported the force needed to fracture the stamp from the template.

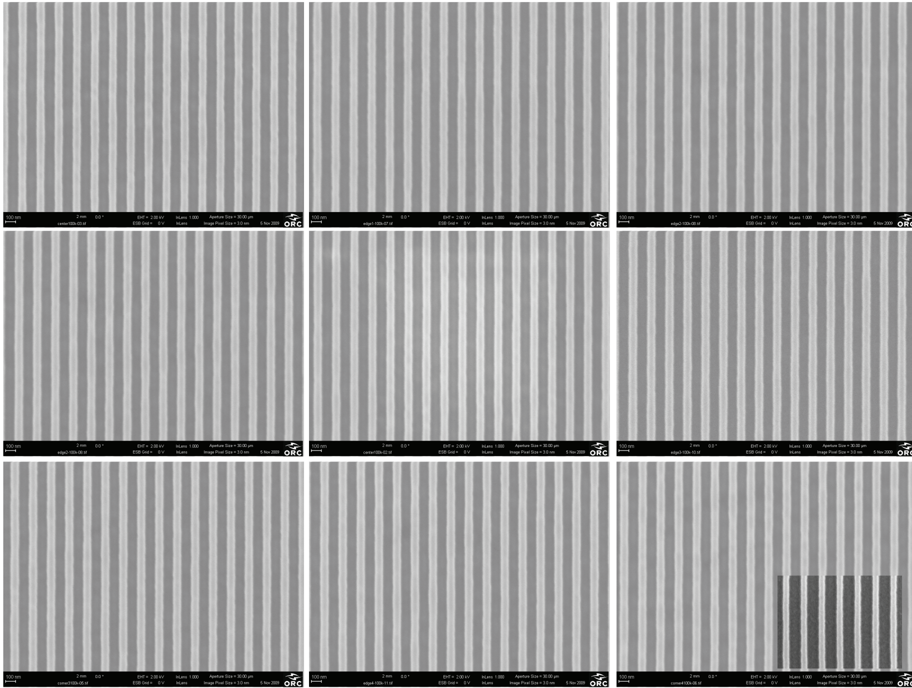

Figure 12. Cytop coated 5 x 5 cm^2 template imaged from each corner, from the centre of each edge and from the centre of the template. The pattern is a grating having a 180-nm period, 45-nm height and 66-nm linewidth. After the Cytop coating the linewidth of the template is 78 nm. The insert in the lower right corner shows a part of the template before coating. The order of the images corresponds to the positions from which the image of the substrate is taken The centremost image is taken from the centre of the substrate, the image in the upper left corner is taken from the upper left corner of the substrate, *etc.*.

Fracture strength was measured for both the patterned and unpatterned templates. It seems that for an unpatterned template FDTS produces release properties nearly as good as Cytop but for the patterned template the Cytop coating has a much lower adhesion to the stamp material. Wear properties of the coatings were not studied since each template was used to make only a small quantity of stamps. Our coatings seemed to be good enough to replicate 10 to 20 stamps from a single template. It was observed that the anti-adhesion coating could be easily removed from the template, and the template could be re-coated in a new anti-adhesion treatment.

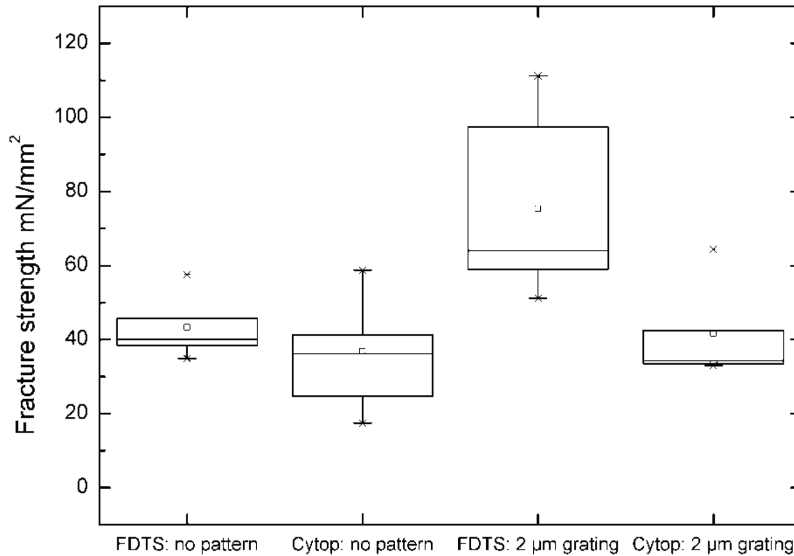

Figure 13. Fracture strength for different experiments. The patterned template had 2-µm lines in 4-µm pitch. The pattern depth was 200 nm [(7)] (Unpublished).

This test series clearly show that the anti-adhesion treatments cannot be evaluated simply by evaluating their contact angles. Both the coatings studied have almost the same contact angle for water (FDTS 107°, Cytop 110°) but the release properties for the patterned surfaces differ significantly. This is because the contact angle test does not treat the friction or the influence of the pattern's sidewall. During the curing, Ormostamp shrinks significantly[(8)] and this causes strong pressure on the sidewall facing the edge of the template. Apparently, for any dense pattern, the sidewalls play an important role. The sidewalls are often rougher than the top surface or the bottom surface. This fact increases the friction caused by the sidewall. We believe that the fluoropolymer coating offers better release properties than the FDTS coating mainly because fluoropolymer smoothens the sidewalls.

[(7)] Vertical line represents the *median* of the data, the square dot the *mean value* and the box shows *25th* and *75th percentiles* (50% of the measurements points fall within the box), while the whiskers show *5th* and *95th percentiles*. The furthest markings refer to maximum and minimum values.
[(8)] Ormostamps volumetrick shrinkage is from 5 to 7 %.

4 Pattern transfer using NIL

We proved in the earlier Sections that NIL is a powerful tool for replicating nanopatterned templates to polymer layers placed on a substrate. In many applications, a pattern from an imprinted polymer layer must be further transferred to underlaying layers or to the substrate. Plasma etching and layer deposition play important roles in the pattern transfer. We may say that most of the time spent on NIL processing is accounted for by plasma processes. This is particularly true when high-aspect-ratio patterns are fabricated. For example, the fabrication of high-aspect-ratio gratings for a DFB-laser diode(9) requires up to five sequential plasma etch steps.

In this Section we discuss pattern transfer by layer etching. We include etching of a silicon nitride (SiN) mask layer and a finding a way to make a polymer layer for a lift-off mask. High-aspect-ratio etching of various III-V semiconductors will also be discussed in great depth, and several illustrative examples are given.

4.1 Residual layer etching

Residual layer etching is an unavoidable step in NIL. Usually, short blanket etching with a reactive ion etcher (RIE) is enough. The blanket etching causes no problems if the imprint has left a thin (5 nm to 20 nm) highly uniform residual layer. However, if the residual layer is as thick as the linewidth, or is non-uniform, the patterns may shrink or vanish.

Non-uniform residual layer reduces process latitude since the target etch depth changes over the imprint field. In the areas where the residual layer is thinnest one needs to over etch. However it is not possible to over etch deeper than the height of the patterns.

(9) presented later in Chapter 5.1

Additionally, if the residual layer is non-uniform, the blanket etching penetrates into the residual layer first in those areas where the residual layer is the thinnest. In these areas the load[10] on the plasma changes, causing a local increase in quantity of etchant. This undesired effect increases the etch rate locally. Since etching cannot occur vertically it may well start to occur laterally. A similar phenomenon is observed if the residual layer is over-etched. As soon as the residual layer is penetrated, the density of reactants increases, since the area consuming the reactants is decreased.

If the residual layer is thick, compared to the linewidth, it is possible that the amount of lateral etching becomes significant. The proportion between vertical etching and lateral etching can be tuned by the process conditions. Our best results with the NIL resist AMONIL (AMO GmbH, Germany) indicated that the vertical etch rate was 5 – 10 times the lateral etch rate. These results were achieved with $SiCl_4$ plasma at a low plasma pressure (3 - 8 mTorr). Our process conditions enabled strong silicon-based sidewall passivation which improved the ratio of the two etch rates.

4.2 SiN mask layer

Patterned SiN layers deposited using PECVD were extensively used in this Thesis as mask layers for subsequent etch steps or as functional layers. We used several ways to pattern these layers. For thin SiN layers, direct etching was possible using a NIL resist as a mask. For high-aspect-ratio patterns, chrome or aluminium was used as an intermediate layer. The advantage of aluminium is that it can be easily stripped off the compound semiconductor wafer after use. For Cr, this is not always possible without damaging the underlying layers; therefore, the thickness of the Cr layer must be carefully calculated in order to allow it to wear off during subsequent etch steps. On the other hand, as shown in Table 5, Cr can be etched with very high selectivity using organic-inorganic AMONIL. Table 5 also shows that although mr-UVCur06 has favourable viscosity for NIL, often the best choice may be AMONIL because of its superior etch resistance to chlorine and oxygen containing plasma. The durable Cr-mask, patterned with AMONIL, allowed the best SiN etch results shown in Figure 14.

---

[10] load refers to the consumption of etching gas

Table 5. Etch rate matrix (nm / min) for SiN and its mask materials. Cr and Al are etched in ICP system and SiN is etched in RIE system.

Material	CHF_3/Ar (SiN-etch)	Cl_2/O_2 (Cr-etch)	BCl_3/Ar (Al-etch)
Cr	1	25	Not relevant
Al	3.2	Not relevant	107 (11)
SiN	72	0.5	42
mr-UVCur06	29	80	204
AMONIL	34	7.4	88

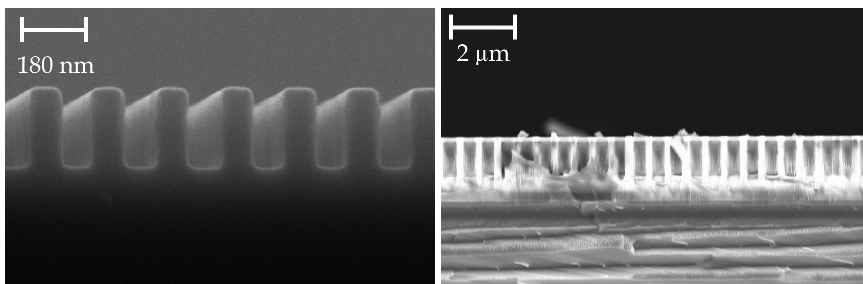

Figure 14. SiN patterns etched with a Cr/AMONIL etch mask. Left panel: 90-nm wide lines in a 180-nm pitch, etched down to 235 nm. These were used as an etch mask in AlGaAs/GaAs etching. Right panel: 1.1 µm deep circular holes, in a square lattice, with a period of 700 nm. Damage in the cross-section image was caused by improper cleaving of a thick silicon wafer.

4.3 Pattern transfer with lift-off

Lift-off is an additive process in which a patterned mask layer is used to define the areas where materials are to be added. For lift-off, it is favourable to use a mask that consists of a *T* -shaped or *V* -shaped cross sectional profile. This pattern profile prevents the deposited metal from covering the sidewalls of the mask. In fact, there are several options to modify the chemical composition of a photoresist in order to prepare a desired pattern profile. None of these options,

(11) Native Al_2O_3 on Al delays etching during the first seconds. During the first 10 seconds only a 9-nm layer is etched but then etching occurs at the etch rate of 107 nm/min.

unfortunately, are available for NIL to date; therefore, one must rely on a properly tuned etching of multi-layer stacks. We have utilized a multi-layer stack consisting of an NIL resist on top, a metal intermediate layer immediately below the resist, and an organic polymer layer as the bottommost layer.

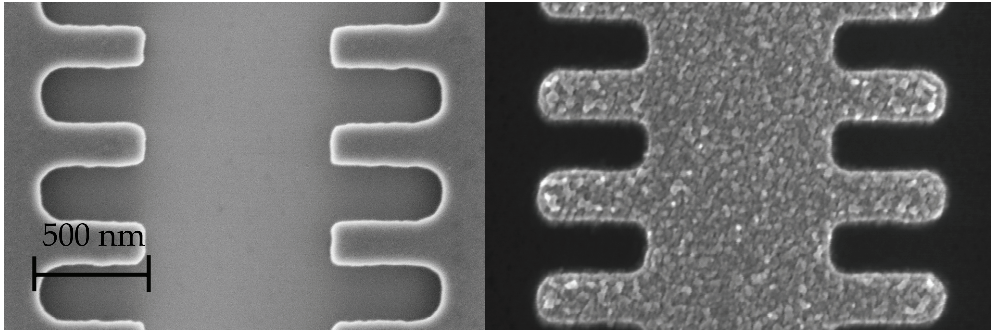

Figure 15. Pattern transfer results from a template (left) to an aluminium layer (right), patterned by means of lift-off. The period of the grating is 450 nm.

Table 6. Etch rate matrix (nm / min) for lift-off process and its mask materials.

Material	CHF_3/Ar	CHF_3/Ar/O_2	O_2
AMONIL	29	74	8
mr-UVCur06	34	200	240
Germanium	3	55	3
PMMA	45	165	320

Table 6 summarizes typical materials used in P3. I employed germanium as an intermediate layer and PMMA as a sacrificial organic layer. This layer stack was chosen because Ge withstands O_2 plasma etching of PMMA. This is important since O_2 plasma etching of PMMA always causes lateral etching which, in turn, induces T-shaped patterns. A thin Ge layer can be easily etched, for example, with CHF_3 / Ar / O_2 or $SiCl_4$ plasma. The pattern transfer process is very effective, and is illustrated in Figure 15 for the case of preparing a periodic Bragg grating, a "nano-comb". We note in passing that our research group has presented high-aspect-ratio lift-off

processes resulting in three-dimensional pattern shapes, using the same masking process (Kontio *et al*. 2009).

4.4 *Pattern transfer to compound semiconductor*

In this Section we introduce the developed dry etching for various semiconductor heterostructures. The demand for high-aspect-ratio etching mainly comes from geometrical requirements when fabricating laterally coupled distributed feedback laser diodes. Edge emitting laser diodes (like DFB-LDs) have a similar p-i-n-diode-like layer structure as illustrated in Figure 16. Light is propagating in the waveguide layer which contains a single or multiple quantum wells for light amplification. The waveguide layer is clad with thick cladding layers to prevent light penetrating into the heavily doped contact layer. In order to make a grating which interacts with light one must etch deep, near the waveguide layer, because light is concentrated mostly in the waveguide.

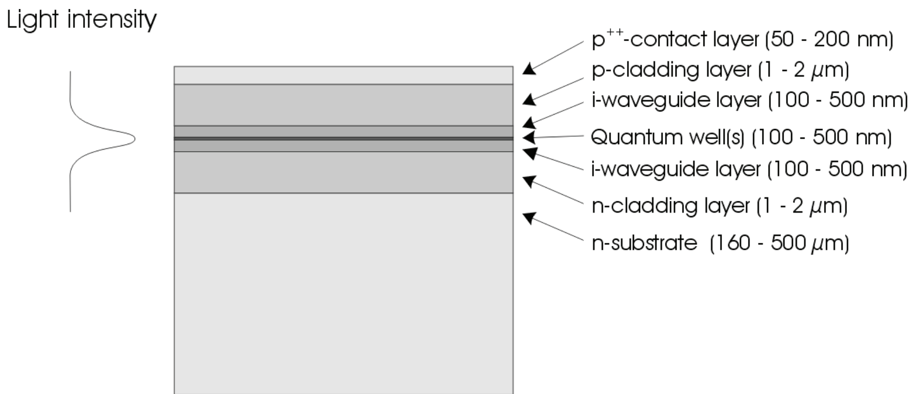

Figure 16. Typical layer structure for edge-emitting laser diode.

This Section shows the results that we obtained with different material systems and compares the results obtained with the state-of-the-art and application requirements. All semiconductor etch steps were carried out in an inductively coupled plasma etch system (ICP) which enables accurate control of the substrate temperature from -150 °C to +400 °C (Oxford plasmalab 100+ having a 4” ICP source).

In addition to these material systems we shall discuss an etch process combining a NIL patterned Al mask and cryogenic silicon etching later in Section 5.3.1.

4.4.1 GaAs/AlGaAs

AlGaAs may be used as a cladding layer in a diode laser, in the spectral range from 650 nm (Sumpf *et al*. 2006) to 1310 nm or beyond (Pessa *et al*. 2003). The AlGaAs layer is capped with a highly doped GaAs layer for low-resistance ohmic contacts to the laser chip. Typical thicknesses of the cladding and contact layers are around 1 µm - 2 µm and 50 nm - 200 nm, respectively. The grating period Λ defined by the effective refraction index n_{eff} of the waveguide, the emission wavelength λ, and the grating order m can be given by

$$\Lambda = \frac{m\lambda}{2n_{eff}} \qquad (2)$$

The period Λ for $650 \leq \lambda \leq 1300$ nm is within the range from 100 to 200 nm if $m = 1$, and longer if $m > 1$. We studied gratings for 180 nm $< \Lambda <$ 450 nm. Our calculations [2, 3] and experiments indicated that the etch depth should be around 1.2 µm for $\Lambda \approx 180$ nm and 1.7 µm for $\Lambda \approx 450$ nm.

We studied several etch chemistries. It turned out that "the best working chemistry" for high-aspect-ratio grating etching was Cl_2 / N_2. $SiCl_4$-based etching was also extensively tested but it was never able to reach the desired etch depth of 1.2 µm for $\Lambda \approx 180$ nm; for the $m = 3$ gratings (Λ = 450 nm) $SiCl_4$ gave satisfactory results.

Figure 17 reveals a correlation between the substrate temperature and the linewidth of the etched structure. It demonstrates that the linewidth is tunable by the substrate temperature during etching. In fact, the temperature plays a key role in sidewall chemistry. Namely, the passivation of the sidewall at room temperature appears to be insufficient to maintain a desired linewidth. The sidewalls eroded during etching; reducing the linewidth (Figure 17). However, at lower temperatures sidewall passivation became strong enough to withstand attacks of chlorine. This observation was due to the fact that chlorine ions were less reactive when the substrate

temperature was low. Remarkably, the linewidth reduction was reproducible, therefore this effect can be used to tune the linewidth.

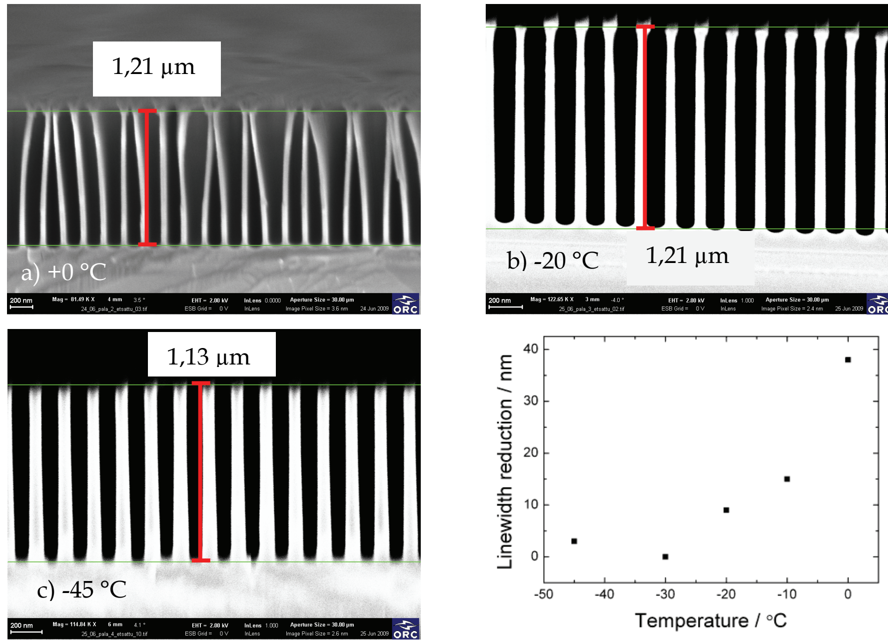

Figure 17. The effect of the substrate temperature on the linewidth of the patterns. Figures a, b and c show the cross section of the grating when etched at different temperatures. Figure d shows the influence of temperature on the linewidth. In all figures the period of the grating is 180 nm, and the etch depth is roughly 1.2 µm (publication under preparation).

Our results demonstrated state-of-the-art results when dense-pitch high-aspect-ratio structures were to be etched in GaAs / AlGaAs. The results reveal a novel etch chemistry, not much studied in the literature. We believe that the Cl_2 / N_2 plasma has other advantages, too, when compared to processes which utilize $SiCl_4$ or BCl_4. Our chemistry is "clean". It does not contain atomic or molecular species that would contaminate the walls of the process chamber. Therefore, it reduces the need to clean the chamber, improving the uptime of the etch tool. Earlier studies, supported by our experiments, on low-temperature etching of GaAs / AlGaAs suggested that low substrate temperatures decreased the etch rate, but improved the etch uniformity and simultaneously reduced the RIE-load effect. The RIE-load effect is harmful because it changes the etch rate when the total area or the density of patterns are changed (Gregus *et al*. 1993).

4.4.2 *InGaAs/InP material system*

An InGaAs contact layer and an InP cladding layer are used for preparing data transfer lasers at λ = 1310 nm and λ = 1550 nm (Tandon *et al*. 2004, McKee *et al*. 1997); of course, InGaAs / InP can also be used for longer wavelengths (Lyutetskiï *et al*. 2003). To prepare the first order grating (m = 1) at λ = 1310 nm, an etch depth of 1.5 µm is required for a Λ = 200 nm period.

In this application we also used Ar-diluted Cl_2 / N_2 plasma, but instead of a low substrate temperature we applied high temperature (200 °C) to increase the etch rate and volatility of the etch products. We were able to demonstrate precisely made m = 2 gratings (right panel, Figure 18) but when m = 1 gratings were fabricated the direction of etching at the bottom of the grating was somewhat random (left panel, Figure 18). In this case etching took place in new directions, slightly to the left or right of the intended vertical direction. At the same time m = 2 gratings had very regular dimensions but the bottom of the groove had an unusual V-shape.

I expect these effects are caused by the increase of crystallographically oriented chemical etching when the aspect-ratio of the grating is high enough. These experiments are made with wafers cut in the (100) direction, while the cross section was cleaved along the (110) plane. In other words, the densely packed and potentially slowly etching (Fiedler *et al.* 1982) (111)-plane is oriented to 54.7° with respect to the surface of the wafer. I believe etching results could be further improved if another wafer orientation and grating direction were used, which would allow us to apply the (111) plane as a sidewall of the grating lines. For this purpose it would be of interest to study InP wafers oriented in the (110) directions.

Recent results by Dylewicz *et al*. (2009), however, give hope that fabrication of m = 1 gratings is conceivable, although more work is needed to find a correct parameter window for the etching. Dylewicz etched a Λ = 236 nm grating down to a depth of 3 µm. This state-of-the-art result was achieved with Cl_2 / N_2 / Ar chemistry, practically the same gas combination as we employed. They also used elevated substrate temperatures. Dylewicz's pattern layout bore a close resemblance to our structure (Figure 15, a "nano-comb"). This kind of pattern layout allowed a

lateral flow of gas away and into the grating; free gas flow might be a significant advantage in high-aspect-ratio etching.

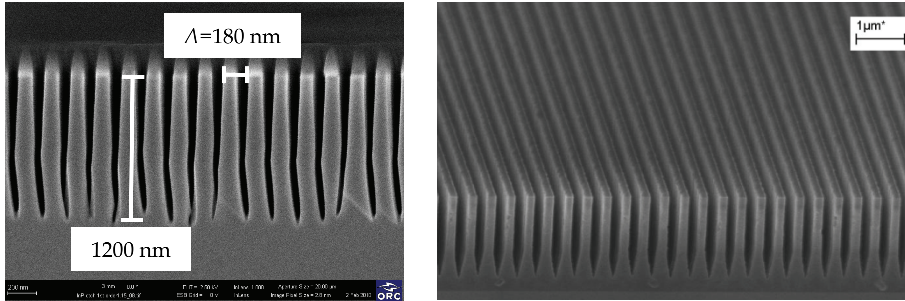

Figure 18. Left Panel: 1.2 μm deep *m* = 1 gratings etched in InGaAs/InP. Right Panel: 1.7 μm deep *m* = 2 gratings etched in InGaAs/InP using a SiN mask fabricated with UV-NIL (right image courtesy of Ligang Deng, Oxford Instruments).

4.4.3 *GaSb/AlGaSbAs material system*

A GaSb contact layer on an AlGasbAs cladding layer has been exploited in the fabrication of an infrared diode laser which emits at 1.9 μm ≤ λ ≤ 3.0 μm at room temperature (Newell *et al*. 1999; Lin *et al*. 2004). The grating pitch for *m* = 1 would start from 270 nm; the required etch depth is roughly 2 μm. This target was considered too challenging for the time being because, to the best of our knowledge, there are hardly any publications available for high-aspect-ratio etching of GaSb/AlGaSbAs which would come close to these dimensions. Therefore, this thesis focuses on *m* = 2 and *m* = 3 gratings.

In our process, mixtures of Cl_2, N_2 and Ar gases were tested at different process parameters. Etching was performed at room temperature. Our results were encouraging (Figure 19); we obtained an etch depth of 1.2 μm for a Λ = 400 nm grating and a depth of 2 μm for Λ = 800 nm. These results can be deemed state-of-the-art. They were achieved with a relatively small effort compared to our long work on the GaAs and InP based materials. This strongly suggests that by putting more effort into GaSb / AlGaSbAs, selected etch chemistry could be pushed to more challenging aspect-ratios and linewidths than what are possible today. This would yield better performance features for GaSb-based devices which are becoming key materials in the mid-IR

range for many applications, for example, for remote sensing of environmentally hazardous gasses.

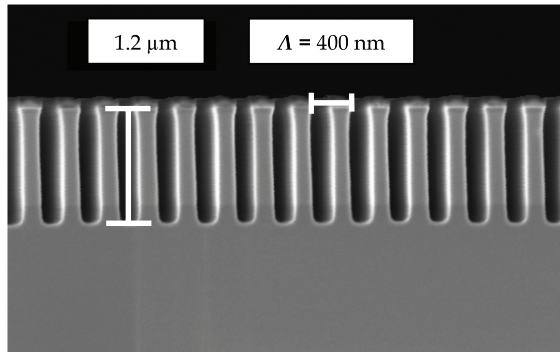

Figure 19. Etched grating into GaSb/AlGaSbAs. Etch depth of the grating line is 1.2 µm and Λ = 400 nm (unpublished).

5 NIL in nanophotonics

In this Section we concentrate on devices which have been fabricated with UV-NIL.

A distributed feedback laser diode (DFB-LD) is one of the devices we have made. DFB-LDs emit a single longitudinal mode with a narrow spectral linewidth and a low frequency chirp. We believe that our work demonstrates the first attempts to make DFB-LDs by soft UV-NIL. In particular, we prepared laterally coupled DFB-LDs. We also show, for the first time, how to realize laterally coupled DFB-LDs together with efficient current injection and high grating coupling.

The second group of devices we shall discuss here are nanopatterned silicon and silicon nitride membranes. The membrane can be used as a sieve or, for example, as an optical filter or a sensor. We have studied how to make large-area membranes quite extensively, and exploited different material combinations. Needless to say this work has required a large amount of nanopatterned wafers but, again, soft UV-NIL has excelled in providing them. We also show a novel way to use these membranes as optical components.

Thirdly, we have worked on epitaxial growth by molecular beam epitaxy on nanopatterned surfaces; a difficult process to master appropriately. One faces a number of problems: how to make extremely small nanopatterns (on a sub-100 nm scale), how to clean the wafer prior to loading it into the epitaxy system, how to clean the substrate surface in the epitaxy system and, finally, how to grow nanopatterns with desired shapes and cover them with high quality layer structures. Clearly, one must make several iterations with various nanopatterns to learn the fabrication process. Once again, we note that NIL has turned out to be a useful method to pattern the wafers since large quantities of identical samples with high resolution patterns must be grown. Understandably, to cover the whole topic falls beyond the scope of this Thesis but I shall briefly review a NIL process to show some of the important results obtained.

Finally, we show that no surface is "safe" from NIL. Section 5.4 illustrates the potential of NIL for the fabrication of a totally new class of functional optical fibres. We show that NIL can be used to pattern a functional element onto the facet of a fibre which alters the properties of light entering or exiting the fibre. We expect that this kind of technology will open possibilities to provide optical fibers with ever more functionality.

5.1 Distributed feedback laser diodes

Distributed feedback laser diodes have cavities with periodic structures, which form a wavelength selective feedback mechanism. The periodic structure in a DFB-LD is a grating embedded within, or at the side, of the waveguide. As discussed in Section 2.5, the linewidths of these gratings are well within the reach of NIL.

The substrates used in the production of DFB-LDs are 2" or 3" in diameter. Therefore, patterning of the full wafer is possible with a single imprint; a large-are imprint, however, prefers a flexible stamp. Wafers of 2" or 3" in diameter are seldom completely flat. Laser diodes, and other optoelectronic components, are grown on substrates which are not as uniform as their large-area prime-grade silicon or glass counterparts. Because total thickness variation (TTV) is between 5 µm and 15 µm for GaAs and InP wafers (Sumitomo 2009), a flexible stamp is desired. Such a stamp can also be easily separated from the substrate because it bends under minimal force, so that a fragile substrate like GaAs, InP or GaSb is not damaged. It is worth noting that the yield of lithographic processes is sensitive to particles present on the surface. Fortunately, the laser chips are small in size, usually (250 – 500) x (250 – 3000) μm^2 in area, and the particle-sensitive waveguide on the laser only covers a fraction of the chip. Therefore, a small number of particles is not a big problem for NIL processes which use a soft stamp. With a hard or non-flexible stamp a single particle could destroy a large number of devices.

We now proceed to investigate laterally coupled gratings and their functionalities. Our components rely on ridge-waveguide type lasers and corrugated ridge sidewalls (Figure 20). The corrugation, if properly made, acts as a good grating. Light propagating in such a waveguide

experiences periodic reflections caused by the periodically changing effective refractive (n_{eff}) index of the waveguide. These reflections generate the distributed feedback.

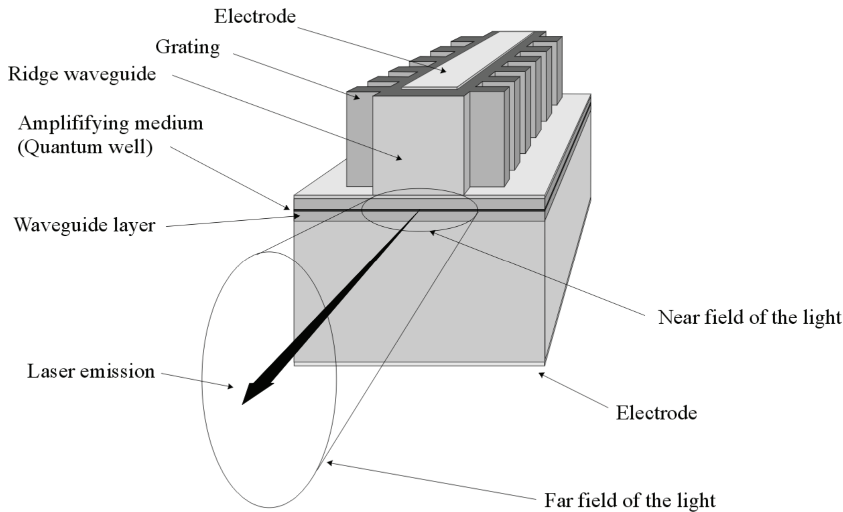

Figure 20. Schematic operation principle of a laterally coupled distributed feedback laser diode.

Laterally coupled laser diodes (Miller *et al*. 1991) are desired for many applications, including quantum cascade lasers (Williams *et al*. 2005; Golga *et al*. 2005), terahertz generation (Pozzi *et al*. 2006), and photonic integrated circuits (Tolstikhin *et al*. 2009). The interest in lateral coupling origins from the fact that DFB lasers with laterally coupled gratings can be made without any layer re-growth. The grating can be applied to any compound semiconductor heterostructure. As a matter of fact, the fabrication of lateral gratings is a slightly modified waveguide fabrication process and easily implemented in photonic integrated circuits. The lateral grating also affords opportunities to vary waveguide dimensions to a large extent, while achieving close control over the lasing mode. We display in Figure 21a a fully fabricated waveguide with a lateral grating placed on both its sides. Figure 21b also illustrates good pattern fidelity over a large wafer area.

A second way to implement laterally coupled gratings is to use metal gratings on both sides of the ridge. The gratings introduce periodic complex-coupling as a feedback mechanism (Kamp *et al*. 2001). Both techniques are rather similar since they allow a re-growth free way to realize DFB-

LD. From the fabrication point of view the metal gratings are rather difficult to fabricate by means other than high acceleration voltage electron beam lithography, since the grating has to reach the edge of the ridge to maximize the coupling. On the other hand, metal grating does not require high-aspect-ratio etching which is somewhat challenging, but possible, as demonstrated in Section 3.

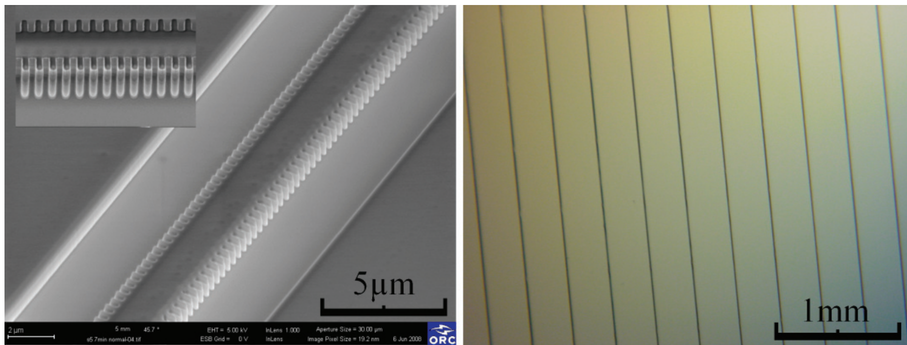

Figure 21. Left panel: Imprinted and etched waveguide for DFB lasers, period of the pattern is 450 nm and etch depth 1.7 µm. Right panel: Microscope image from DFB-laser diode wafer after the imprint.

There are significant challenges for the fabrication of devices by NIL. Among them are the ways to imprint the waveguides, which have wide and isolated patterns. Another challenge is to etch high-aspect-ratio patterns. Our reference (P3) discussed imprinting wide waveguides in such a manner that no pattern corrections were needed; this too is an important issue in NIL.

Deformation of the stamp, resist viscosity and stamp geometry all play a role when making attempts to minimize the residual layer thickness. However, as discussed earlier, the waveguide layout (Section 3.2) and polarity(12) (P4) are also important. The first devices were made by lift-off, as described by (P3). Later on we changed the processes to direct etching of a Cr/SiN-mask. We found out that direct etching offers better polarity for low residual layer imprints and required less process steps.

(12) Polarity: Any patterns on the template can be defined either by etching the pattern itself or alternatively its surrounding

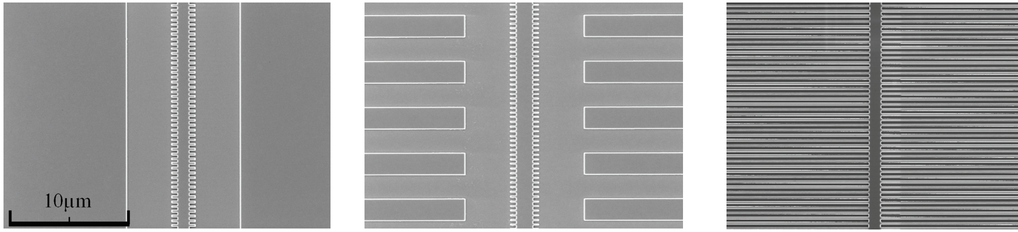

Figure 22. Three different layouts for laterally corrugated DFB-LDs. Left panel: “nano-comb”, centre panel “corrected nano-comb” and right panel “long nano-comb”.

We tested three corrugated waveguide layouts (Figure 22), which we call a “nano-comb”, a “corrected nano-comb” and a “long nano-comb”. When we used the “nano-comb” layout and direct etching of the etch mask, we achieved a residual layer thickness of AMONIL of 120 nm, while a thickness of 175 nm was obtained by lift-off. The “corrected nano-comb” reduced the residual layer significantly, as shown in Figure 10, but the smallest achievable value was not tested since the “long nano-comb“ was more promising, exhibiting good compatibility with NIL and improving etching results, as explained later.

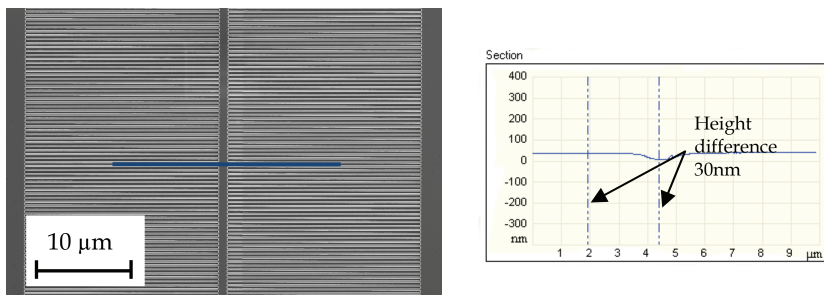

Figure 23. Left panel: Finalized layout for a laterally coupled DFB ridge with long nano-comb. Line indicates the position of AFM scan. Right panel: Atomic force microscope micrograph showing close up of the ridge section in the imprinted resist. Deformation is only 30 nm at the centre of the ridge, and the grating looks perfectly filled with resist. Dashed vertical lines indicate points where measurements are taken.

With the “long nano-comb”, a thin residual layer was obtained when the spin-coated layer was little (~10 nm) thicker than one half of the depth of the pattern on the template. Since the fill factor of the grating, defined by the ratio of the etched area to the non-etched area, was 0.5, this thin resist was just about enough to fill up the patterns in the stamp, leaving behind only a sub-10-nm residual layer. In other words, we could accurately transfer the patterns from the

template to the substrate and maintained a very uniform and thin residual layer. It should be noted that little deformation took place in the centre of the waveguide (see the right panel of Figure 23). There was a slightly insufficient amount of resist to completely fill the area, yet such a pattern deformation had no influence on the etching steps. In the areas having no patterns at all, the thickness of the resist remained unchanged during imprinting.

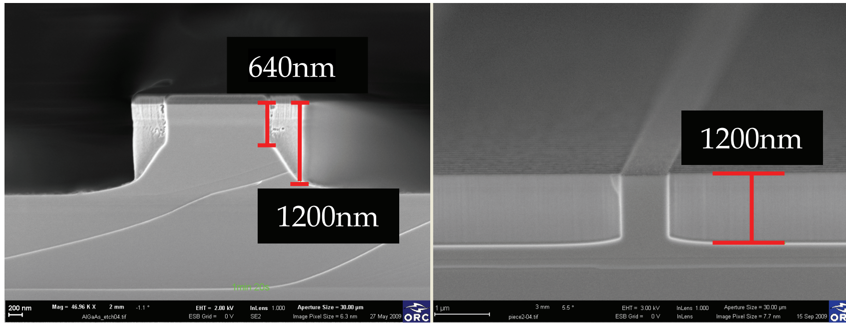

Figure 24. Left panel: Scanning electron microscope images showing the effect of aspect-ratio-dependant etching for a "nano-comb" layout. Right panel: SEM image showing nearly perfect etch profiles for the "long nano-comb".

The difference between the "nano-comb" and the "long nano-comb" layouts have a remarkable impact on etching. The problem in the "corrected" and "uncorrected nano-comb" designs is that the waveguide is isolated by a several micrometers wide groove, which should be etched at the same time as the nanoscopic structures. As the aspect ratio of the nanoscopic structures increases rapidly during etching, the etch rate decreases. Aspect-ratio-dependant etching occurs because flow resistance (of etchant and etch product) to the bottom of the pattern increases when the aspect-ratio increases, which reduces the reaction rate. At the same time, the microscopic structures are being etched at a constant rate since their aspect-ratio is small. As a result, the microscopic structures are etched deeper than the nanoscopic structures. Gas may also flow laterally. This is the main reason why in Figure 24a the etch depth gradually changes from 640 nm to 1200 nm. This non-ideal etch profile (in Figure 24a)reduces the coupling coefficient (κ) [(13)] of the grating and makes it difficult to predict accurately the numerical value of coupling. The waveguide with the long grating lines (Figure 24b) does not have such a problem since the layout contains only patterns with equal linewidths. As a consequence, the κ of the grating can

[(13)] The amount of coupling per unit length between two counter propagating waves in a cavity

be increased, and it is easier to model coupling between the fundamental transverse mode and the grating.

Unfortunately, extending the gratings generates a current spreading problem. This is because the portion of the current spreading outside the area of the fundamental transverse mode does not contribute to the modal gain of the fundamental mode, decreasing the lasing efficiency.

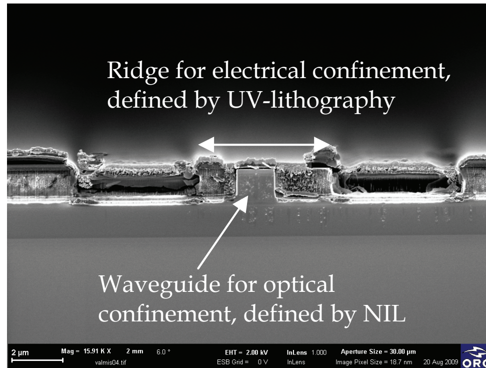

Figure 25. Cross section of the DFB waveguide, defined by a two-step lithographic process including passivation and metallization.

We implemented a current confining structure by etching a second ridge on both sides of the waveguide. The etching of this ridge was rather difficult since the process had to be executed in two steps. In the first step, we defined a transverse waveguide and long grating lines by NIL, as illustrated in Figure 24b. Subsequently, the UV-photolithography step was implemented to define the ridge for current confinement. This approach required precise alignment of the current confining ridge. Due to limited alignment accuracy, the current injection into the fundamental transverse mode may be non-uniform if the current confining ridge is misaligned. The resulting waveguide structure is shown in Figure 25.

5.1.1 *DFB lasers at 975 nm*

We started the work on DFB-LDs by studying λ = 975 nm lasers. The layout of our early waveguides had an uncorrected nano-comb. This approach, although incomplete, allowed us to demonstrate the world's first DFB-laser, fabricated by UV-NIL.

The 975-nm laser diode contained three InGaAs quantum wells embedded in a GaAs waveguide. The waveguide had an $Al_{0.6}Ga_{0.4}As$ cladding layer and a heavily doped GaAs contact grown on top of the cladding. We used an m = 3 grating (Λ = 450 nm) to keep the aspect-ratio of etching at a reasonable level (around 7.5). These lasers exhibited a high side-mode suppression-ratio of 50 dB near the gain-grating resonance, and 40 dB across the tuning area of 3 nm. The devices exhibited a wavelength tunability of 77 pm/°C due to the temperature dependence of the n_{eff}. The continuous wave (CW) light-current-voltage relation and the spectrum of such a device are shown in Figure 26.

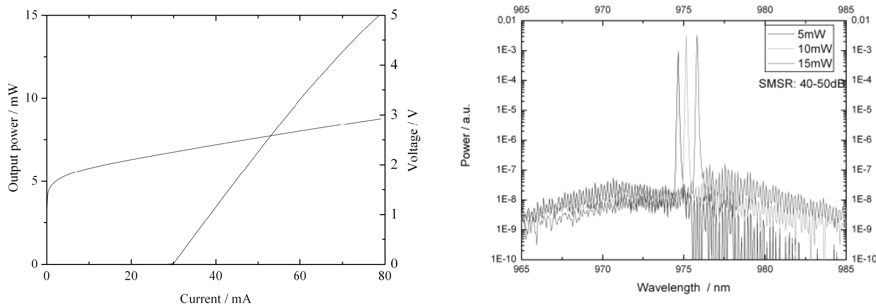

Figure 26. Left panel: CW light-current-voltage behaviour of the anti-reflection/high-reflection -coated DFB laser exhibiting a threshold current of 30 mA and a slope efficiency of 0.35 W/A. Right panel: Spectrum of the device measured at 5 mW, 10 mW and 15 mW output power (Viheriälä *et al*. 2009).

Due to the non-ideal etch profile the 975-nm laser had low κ and did not operate as a DFB-LD across a wide temperature range, nor did it lock with the grating unless the gain and the grating were in very close resonance.

5.1.2 *DFB lasers at 894 nm*

The λ = 894 nm DFB lasers were designed for exciting the D1 line of a caesium atoms. These lasers are intended for atomic clocks of satellite positioning systems, where side-mode suppression-ratio (SMSRs) over 25 dB, moderate light output power of about 15 mW, and narrow emission linewidths of 1 MHz or smaller are required. Our devices had a single GaInAs quantum well embedded in a GaInP waveguide. The waveguide also had an $Al_{0.7}Ga_{0.3}As$ cladding layer and a heavily doped GaAs contact layer grown on top of the cladding. In the first approach we prepared the lasers using the same layout as that of the 975 nm DFB-LD. Grating periods were Λ = 418.6 nm and Λ = 421.4 nm (m = 3), which produced resonances with the cavity field at λ = 888 nm and 894 nm, respectively. The wavelength could be tuned by 89 pm/°C by varying the chip temperature. Figure 27 displays CW light-current-voltage curves and emission spectra for one such laser.

Our 894-nm DFB-LDs exhibited higher efficiencies than the 975-nm lasers, due to a closer optimization of the heterostructure. DFB operation was maintained across a wider temperature interval since emission from the 894 nm quantum wells red-shifted much less than did the 975-nm quantum wells. As temperature was varied the shift was 0.222 nm / °C for the 894-nm device *versus* 0.331 nm/°C for the 975-nm device. The tuning range was, however, just about 2 nm for the 894.6-nm laser. The cavity of this laser was made relatively long, 1.8 mm, to provide satisfactory coupling between the weak grating and the fundamental mode. To achieve satisfactory coupling we etched all the way down to the interface between the waveguide and the *p*-cladding layer, measured from the area around the gratings. The deeper etch could improve the coupling but it dramatically decreased the efficiency of the laser because of the damage etching caused to the waveguide.

Lasers with the “long nano-comb” layout and the current confining ridge demonstrated significant coupling (κ = 22 cm^{-1}), as illustrated in Figure 28. For a relatively short cavity of 0.55 mm we demonstrated broad wavelength tuning of 5.5 nm by varying the chip temperature between 10 °C and 100 °C. Higher temperatures than 100 °C were not tested although they could have further improved these excellent results. The slope efficiency was low. This indicated that the field was strongly confined inside the cavity. To the best of our knowledge strong locking

has never before been demonstrated using laterally index coupled DFB-LDs. Actually, the κ with other layouts of ours was always so small that we could not measure its value.

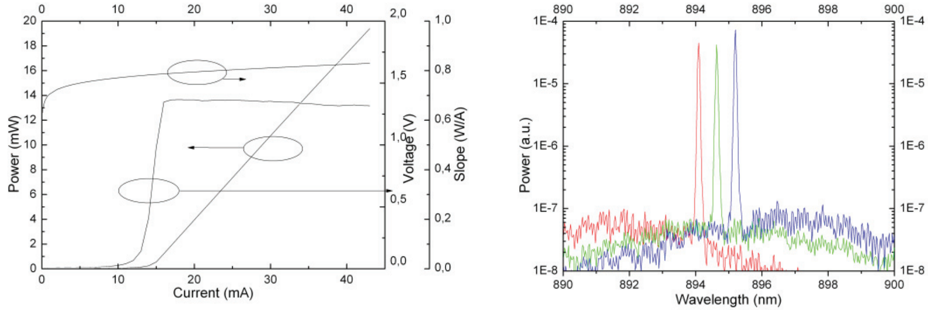

Figure 27. On the left: light-current-voltage behaviour of the anti-reflection/high-reflection -coated DFB-laser diode showing threshold current of 15 mA and slope efficiency of 0.7 W/A. On the right: Spectrum of the device showing the tunability around the D1 transition of Cs-atoms (Telkkälä *et al*. 2009).

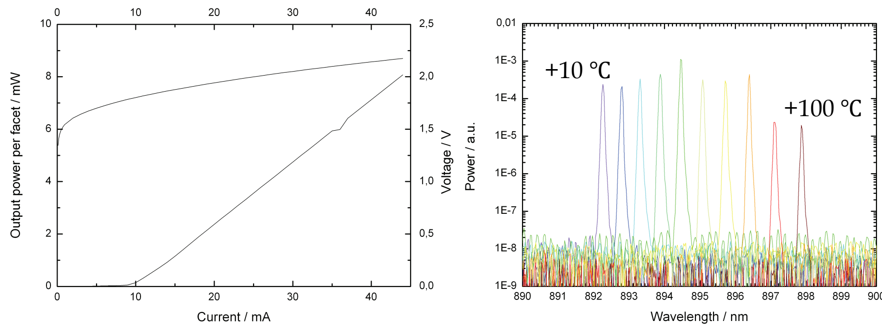

Figure 28. Performance of an 894.6 nm DFB-laser diode with a long nano-comb and a current confining ridge (CW, uncoated facets). Right panel: Spectra in the right panel are measured at temperatures from 10 °C to 100 °C with 10 °C increments. This device shows 40 dB SMSR (publication under preparation).

We chose the cavity length of 0.55 mm to keep the coupling coefficient multiplied by the device length, within the "recommended" limits between 1 and 2 (Henry 1985). For a shorter cavity κ could be improved further because there is room to etch 150 nm deeper before etching reaches the waveguide layer. We should also note that a smaller grating order m would improve coupling.

5.2 *Nanopatterned templates for epitaxy*

In this work, our motivation to pattern the templates before III-V epitaxy was to enable precise positioning of individual quantum dots (QDs). The "standard" method to grow quantum dots is to use the layer-then-island (Stranski–Krastanow) growth mode where growth of a strained layer is followed by growth of a layer that self-assembles into small islands. These islands (or quantum dots) have a smaller band gap than the surrounding material: they can confine electrons in three dimensions. This three-dimensional confinement in a small lateral dimension leads to atom-like discrete energy levels. The disadvantage of self-assembled growth, for many applications, is the random positioning of the dots and their inhomogeneous size distribution.

If one could precisely control the size and the position of the dots, for example, by means of lithography, it would allow the fabrication of many new interesting devices. For example, one could realize quantum dots in a well-defined lattice; this would allow periodic gain media for frequency stabilized lasers. A uniform quantum dot size would lead to a lower threshold current of the laser. The ability to control the size distribution of the dots would lead to control of the gain spectrum of amplifying or absorbing media. In particular, a precise positioning of one or several quantum dots in a cavity could be the foundation of a light source that would emit a single photon or an entangled pair of photons.

Selective epitaxy is one way to allow position selective growth. The idea behind this process is to deposit and pattern a layer of cover material onto a semiconductor substrate. Semiconductor does not stick to this layer during epitaxial growth. The sample, before and after growth, is illustrated in Figure 29. Ideally, this cover material has a low sticking coefficient. Atoms migrate long distances on the surface until they stick to the semiconductor. The material is chemically inert and withstands high temperatures. It can be deposited without damaging the semiconductor lattice and without causing impurities, and it is possible to pattern the layer at a high lateral resolution. We tested selective epitaxy on SiO_2. It worked well and promoted selectivity under correct growth conditions (P7).

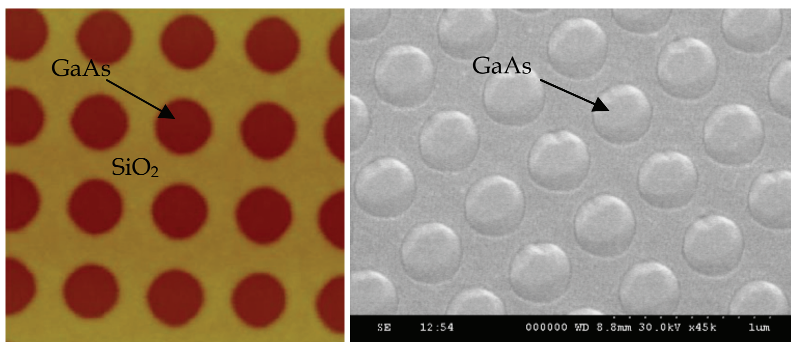

Figure 29. Left panel: Atomic force microscope micrograph of a hole pattern in SiO_2 deposited on GaAs before epitaxy. Right panel: After growth, GaAs appears to have grown only to sites where SiO_2 was removed.

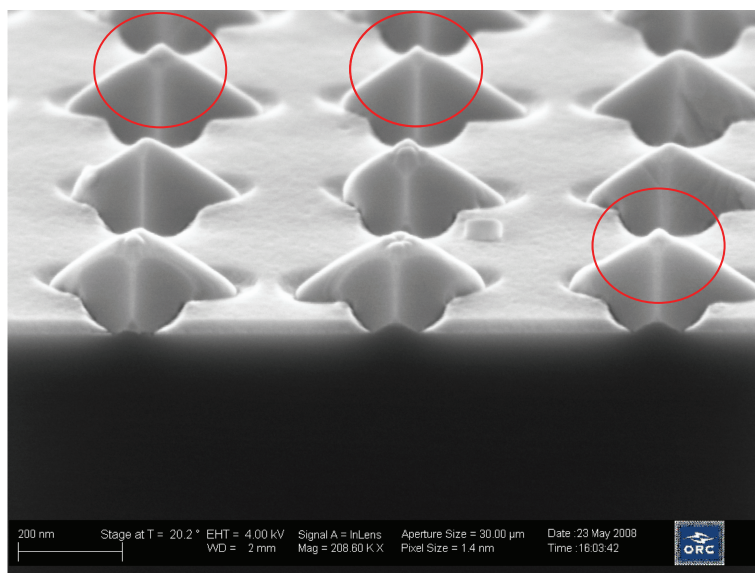

Figure 30. SEM after dual step growth. Initial pattern was a cross: Linewidth 100 nm, line length 400 nm. Pyramids with a single dot have been circled (Tukiainen *et al*. 2009).

To localize QDs we also used holes in SiO_2. The holes were much larger than the quantum dots. The first step in growth was to deposit a thick buffer crystal under conditions which promoted crystallographically oriented growth. The aim of this step was to form a semiconductor island with a sharp apex. The second step was to grow a QD on the apex. This approach was quite successful; it localized the QDs with a reasonable probability. Figure 30 shows a sample after the

growth. We see here that a single InAs QD has been localized at the apex of a pyramid in three places out of nine. Three other sites have multiple dots. Three pyramids have no dots at all.

The problem of selective re-growth is in its complexity. To make any device one has to remove the sample from the epitaxy chamber after QD growth, remove SiO_2, and then make a second re-growth to finalize the wafer for subsequent processing. Because of the complexity of selective re-growth we started to study a localization method where no foreign material was left on the epi-wafer during re-growth. In this approach a small post or a hole was etched into the semiconductor, after which the wafer was carefully cleaned and loaded into the molecular beam epitaxy reactor. Once a thin buffer layer was made we expected that the etched shape would still be visible on the wafer. This application required the smallest patterns used in this Thesis. For the re-growth, we tested pillars and holes having diameters of 40 nm. Compared to the posts, the holes seemed to promote better localized growth of the InAs quantum dots. Figure 31 illustrates patterns before and after the re-growth. Arguably, growth and cleaning of the substrate were not fully successful because one could see some holes in the buffer. However, it is clear that the patterned hole promoted localization of the QD better than the post did. Actually, the QD preferred to grow into a ring that surrounds the post.

Further work on holes that were etched into semiconductor produced improved quality. In an improved series of experiments, a slightly denser pattern and a larger hole diameter (90 nm) were used. Also, cleaning and degassing processes were improved. An atomic force microscope graph (AFM) of the QDs is displayed in Figure 32. Here, more than one half of the holes possess a dot, and the dots are periodically positioned. Further improvement in positioning accuracy is expected under more optimal growth conditions.

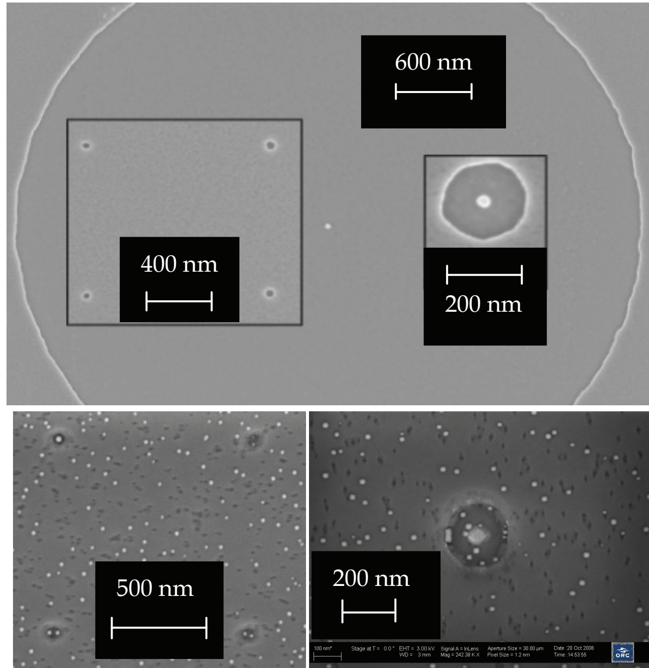

Figure 31. Top panel: SEM image from wafer before the growth. Lower left panel: Growth on the holes etched on the wafer. Lower right panel: Growth on the posts etched on the wafer.

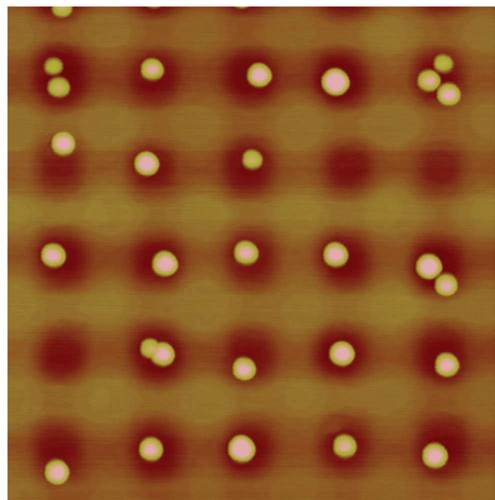

Figure 32. AFM micrograph from the dots grown on a NIL-patterned substrate. Holes are in a square lattice having a period of 180 nm.

5.3 *Nanopatterned membranes*

We studied the fabrication of nanoperforated free-standing membranes and their applications as nanosieves or optical filters. Figure 33 shows schematic cross-sections of nanopatterned membranes. We utilized silicon-based processing because many Si processes were readily available. For this application, high-etch-rate dry and wet etching recipes and stress-free membrane materials were important. Silicon-based components could also be integrated with other silicon chips cost-effectively. Silicon offers the lowest cost per area of all single crystal semiconductors.

The main motivation for investigating the membranes was to demonstrate the sieves' ability to allow diffusion of air through the membrane, while preventing particles with known sizes from penetrating the membrane. It is obvious that the nanoperforated membrane acts as a sieve but the challenge is to make such a membrane. One of the requirements for the membrane is a relatively large area (5 x 5 mm^2). We chose two different material platforms for testing: $Si/SiO_2/Si$ [(14)] and SiN/Si.

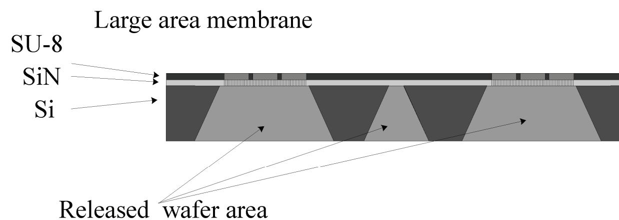

Figure 33. Schematic cross section of wafer containing patterned membranes. Here the nanosieve is fabricated from SiN on a silicon wafer. An alternative membrane could be fabricated from a SOI-wafer.

(14) silicon on insulator (SOI) –wafer

5.3.1 *Silicon-on- insulator based sieves*

Silicon-on-Insulator (SOI) wafers facilated the use of silicon dry etching, which is a well controlled, high throughput process, as demonstrated several times in the literature. The SOI wafers allow for the use of a single crystal silicon layer on top, a so-called device layer, which acts as a nanosieve. The device layer is durable and defect-free. Buried oxide (or BOX for short) acts as an etch stop for release etch and for high-aspect-ratio nano-etch. We learned, however, that for the thick device layer, required by our application (*i.e.*, 2 to 5 µm), the thickness uniformity of the device layer was poor. Variations in the layer thickness of fusion-bonded SOI wafers are remarkable (typically 0.5 - 1 µm), which is to say that SOI wafers would be good only for membranes that are much thicker than what we need. On the other hand, for other technologies producing uniform device layers, the required device layer is too thick.

For high-aspect-ratio etching we used cryo-ICP etching with SF_6-plasma[15]. The etch mask was a 50 nm thick aluminium layer. AMONIL resist was used to pattern the aluminium layer by $SiCl_4$-plasma. Actually, a much thinner layer than 50 nm would have worked well. The Al layer did not show any signs in erosion in a 5.1-µm deep high-aspect-ratio Si etch (Figure 34). We employed a template, which had holes of 350 nm in diameter, in a square lattice with a period of 700 nm.

Results from 5.1-µm deep and 2.7-µm deep Si-etches are shown in Figure 34. The 5.1-µm deep etch resulted in too large dimension shrinkage; as opposed to the case of the 2.7 µm etch which looked rather ideal. We found that non-uniformity in the thickness of the device layer cannot be compensated for by over-etching, because it rapidly leads to significant lateral etching in the device layer – BOX interface. In the SOI process the same cryo-ICP etch recipe was used to release the membranes and to etch the nanoholes. Unfortunately, this way TWV size control was rather poor and the etch rate was low. The advantage was that membranes were released with high yield.

We also demonstrated a method which reduced the perforation diameter by applying atomic layer deposition (ALD). ALD enables conformal deposition of layers on substrates which may

[15] Etching was done by Dr. Lauri Sainiemi from Helsinki University of technology, Micronova, Finland. He used a similar Oxford Plamalab 100 ICP-system as we did for high-aspect-ratio GaAs, InP and GaSb etching.

have an extremely high aspect ratio. Because ALD is a self-regulatory, atomic layer-by-layer deposition mechanism, the thickness control of a deposited film is excellent. Results from perforation size-tuning are discussed in (P5). Our arrays of membranes were 400 x 400 µm^2 in size; larger membranes were not tested.

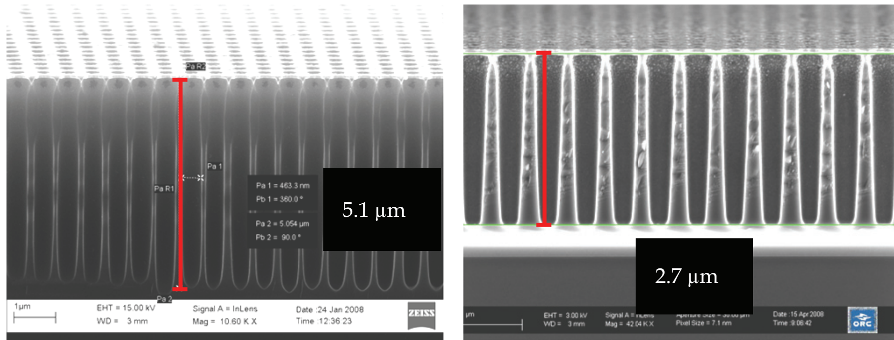

Figure 34. Left panel: 5.1-µm deep silicon etch. The test has been performed on a silicon wafer (no buried oxide or device layer). Right panel: 2.7-µm deep silicon etched in a SOI wafer. Etching has reached the BOX layer, shown as a white layer below the patterned layer. Images courtesy of Dr Lauri Sainiemi.

5.3.2 *Silicon nitride-on-silicon based nanosieves*

Another material system in our experiments was a stress-free nanoperforated SiN film on a Si wafer. The advantages of this material system over SOI are the facts that the SiN film is more uniform than the device layer of the SOI-wafer, and over-etching of SiN does not cause lateral etching since polymer deposition during CHF_3/Ar etching strongly passivates the sidewalls. Disadvantages of thick SiN films (grown by PECVD) are a low etch rate and mask selectivity in RIE. Growing thick films by PECVD is also somewhat impractical.

Even if SiN deposition itself did not take too much time (P6), standard operating procedures of PECVD were cumbersome for thick films. Our PECVD system (Oxford plasmalab 80+, Oxford Instruments) requires cleaning for every 2 µm of deposited film, and vacuum-cleaning for every 6 µm. Failure to follow these instructions leads to particle deposition during PECVD deposition. Moreover, RIE-etching of the SiN film had quite a low selectivity for the Cr layer which we used

as an etch mask. The SiN etch rate was low for deep high-aspect-ratio structures; the time required to reach a depth of 1.5 μm was 45 min. Nevertheless, using plasma instruments properly designed for depositing and etching thick SiN films, these problems could be alleviated to a large extent.

For nanopatterning SiN we employed the same template and the same process flow as nanopatterning the SOI wafers. The only difference was the replacement of the aluminium film by a thicker Cr layer (50 nm to 150 nm). Cr withstands SiN etching better than Al (see Table 5) and with AMONIL it was possible to pattern thicker Cr layers than Al layers. SiN etching was performed in RIE using CHF_3/Ar plasma.

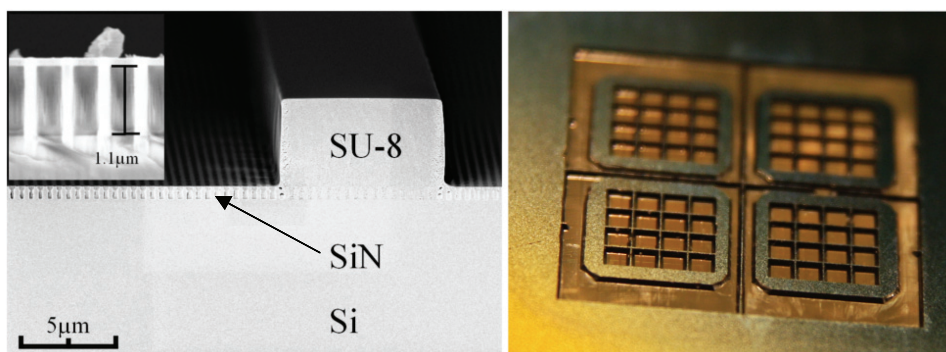

Figure 35. Left panel: SEM image shows a SU-8 support bar and a nanopatterned SiN film. Insert: Close-up of a SiN film after dry etch. Right panel: Image from the backside of the wafer after the release etch. This photograph shows four chips, each having 16 nanopatterned membranes.

The fabricated membranes were released by removing the substrate beneath the patterned area. This was done by anisotropic wet etching in the <100> plane using KOH:H_2O solution (30 % at 80 °C). The large-area membrane was reinforced with a network of epoxy-based photoresist (SU-8, *Microcehm Corp., USA*) supports that divided the large-area membrane into 100 x 100 μm^2 cells. Each cell was supported at its edge by 10 μm wide and 5 μm thick SU-8 bridges. The composite SiN/SU-8 structure allowed us to make 5 x 5 mm^2 free-standing membranes. We also released chips from the wafer simultaneously during the KOH etch. This enabled us to avoid sawing of the wafer, since sawing could damage the membranes. Figure 35 shows a nanopatterned membrane, the SU-8 support bar and four released membrane chips.

5.3.3 *Membranous optical elements*

During the course of the work we believe we opened a new way to integrate optical fibers with nanopatterned membranes on a silicon wafer. Our approach, illustrated in Figure 36, utilized a through the wafer via (TWV) into which the optical fiber could be inserted. On the front side of the wafer we processed a membranous optical element which interacted with the light beam entering into or exiting from the optical fiber. The distance between the membrane and the facet of the fiber could be controlled by standard silicon wet etching techniques. The fiber could be permanently glued onto the TWV. In our case, glue was also used as an index matching medium to eliminate the Fabry-Perot cavity forming between the fiber facet and the membrane. The other challenging requirement was the small size of the holes and the high aspect ratio.

Our demonstration device is based on nanopatterned SiN membranes which act as an optical filter. The filter utilizes guided-mode resonance in a SiN membrane. The filter is composed of a grating placed on top of a waveguide to couple light in and out of the waveguide. At selected wavelengths the waveguide modes couple with the grating and form sharp resonances in reflection and transmission, which are useful for optical filtering and sensing (Magnuson and Wang 1992). Since the area of the filter is rather small it does not require any additional mechanical support which could hinder its optical performance. The guide-mode resonator is composed of a 400 nm SiN film and a 100 nm deep grating. The grating on the membrane had a period of 400 nm and a fill factor of 0.5.

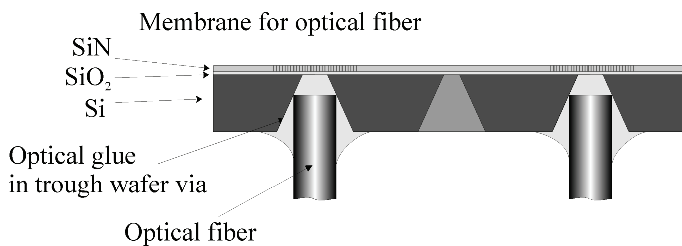

Figure 36. Schematic cross section of wafer containing patterned membranes for optical applications.

We also demonstrated a novel way to position an optical fiber with the filter in order to launch and collect light from the nanopatterned membrane outlined in Figure 36. The fiber can be inserted and glued onto the TWV. This allows seamless and straightforward integration of the fiber and the membranous optical element. To prevent flowing of glue through the penetrated film it is possible to deposit a SiN film on a thin SiO_2 layer on silicon. The device utilizing a SiO_2 backing layer is illustrated in Figure 36. The SiO_2 layer, optical glue, and the fiber core have the same refractive index (~1.46). This is important in order to eliminate Fabry-Perot effects occurring between the fiber facet and the membrane.

The coupling losses α, exhibited by the beam exiting from the fiber, reflecting from the filter and re-entering the fiber, can be estimated from a coupling loss equation for two butt-coupled fibers, separated by a distance d, and surrounded by a medium having a refractive index n_0. For this coupling scheme the separation between the facet of the fiber and the membrane is $d/2$. In equation (3) w_0 refers to the mode diameter of the optical fiber:

$$\alpha = 10\log\left(1 + \left(\frac{d\lambda}{2\pi n_0 w_0^2}\right)^2\right) \quad (3)$$

Eq (3) does not take into account the mode misfit that exists between the fiber and the beam reflected from the nanopatterned surface. The equation predicts that coupling losses are small if the fiber is brought into close proximity with the membrane.

Alignment of the fiber in the TWV should be carried out actively, while the shape of the TWV helps to find a starting point for active adjustment. In our demonstration (P5) we measured *in situ* intensity of the reflection at the resonance to maximize the alignment accuracy. The size of the TWV at the front side of the wafer was 88 x 88 μm^2; therefore, it could be estimated that the distance between the fiber and the membrane was 25 μm when the fiber was optimally aligned. The fiber and the membrane can be brought closer to each other by increasing the TWV diameter. The process is controlled accurately since all of the geometrical parameters are precisely specified. These parameters are: a total thickness variation of the wafer (< 1 μm), the diameter of the fiber (*i.e.* 125 μm ± 0.7 μm for Corning SMF-28), and the precision of

photolithography (< 1 µm). The thickness of the wafer may vary significantly within the wafer batch (±5 µm or more).

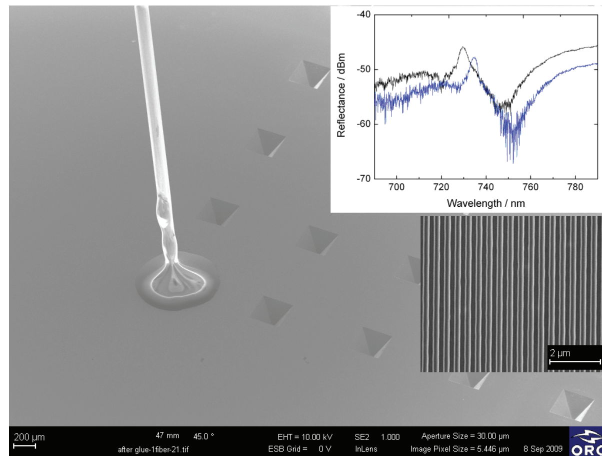

Figure 37. The fiber is aligned and glued into one of the TWVs. Large insert: reflectance spectrum of the optical resonant filter measured from the fiber. Small insert: Close up of the grating of the optical filter on the front side of the wafer.

Once the fiber was aligned we cured the glue with UV-light and tested the membrane's potential as a refractive index sensor. Broadband (500 nm – 1600 nm) light from a supercontinuum laser source (Fianium Inc.) was launched into the membrane through the optical fiber. The light reflecting from the filter was collected by the same fiber and directed to an optical spectrum analyzer through a fiber coupler. The first reflection from the filter was measured when the filter was in air. To investigate the effect of the surrounding refractive index on the resonance wavelength the grating was immersed in water. Reflectance spectra are shown in the insert of Figure 37. The resonance was observed to red shift by 5.1 nm due to the higher refractive index of water (n=1.33). This shift of 15.5 nm per refractive index unit (RIU) demonstrates the possibility to apply this configuration as an optical refractive index sensor. The amount of wavelength shift is comparable to that in a sensor based on a fiber Bragg grating (6.5 nm/RIU demonstrated by Liang et al. 2005), or on a micro sphere resonator (30 nm / RIU demonstrated by Hanumegowda et al. 2005). On the other hand, sensors based on the use of long period fiber Bragg gratings show much higher sensitivity (1000 nm / RIU demonstrated by Bhatia and Vengsarkar, 1996). Slanted fiber Bragg gratings, using a surface plasmon resonance for increased

sensitivity (and losses), have show an extremely high sensitivity of 3400 nm / RIU (Allsop et al., 2007). In comparison, our method offers simultaneously a good platform for integration, low losses and an ability to detect very small fluid volumes down to one pL.

5.4 Patterned facets of optical fibres

Micro- and nanopatterned surfaces of an optical fibre can operate as miniature optical elements. They can modify the propagation of light by diffracting, collimating, shaping, or focusing it. A properly designed optical element on the facet of an optical fibre improves the functionality of the fibre without compromising the compactness of an optical system. Miniaturized elements could subsequently be used for building miniature spectrometers, sensors, and other devices. However, until now suitable nano- and microfabrication methods that would allow for volume production of patterned fibers were non-existent.

So far, a simple optical element that can be prepared on the tip of a fibre is a lens. The lens may be made by grinding or melting the end of the fibre, or by combining segments of fibres with different refractive index profiles (Shiraishi *et al*. 1997 and Yeh *et al*. 2004). More complex elements containing small features are made by micro- and nanopatterning using focused ion beam lithography or electron beam lithography (Giannini *et al*. 2000, Schiappelli *et al*. 2003). These direct writing methods are good but expensive to deploy and capital investments are high. Moreover, their use for any small substrate, such as the facet of an optical fibre, is challenging.

We have demonstrated the world's first surface reliefs fabricated by NIL on the facet of a single fibre (Viheriälä *et al*. 2007). I also believe that this experiment provides evidence for NIL being able to pattern very small surfaces that have not yet been reachable by other nanofabrication methods (with the possible exception of focused ion beam writing). The method utilized a UV-curable polymer which was deposited onto the facet by dip coating. Although dip coating delivers a rather non-repeatable quantity of polymer onto the facet, due to the small size of the fibre, it is possible to press any excess low viscosity polymer away from the facet. This application only requires a simple imprint setup, illustrated in Figure 38. The set-up is built on an optical table. It includes a stamp holder and a micromanipulator for bringing the fibre and

the stamp into contact. A microscope was used to monitor the contact between the stamp and the fibre *in situ*, since excess contact force easily bends the fibre between the fibre chuck and the contact point. The polymer between the fibre and the stamp was cured with a fibre-coupled UV-source delivering immense UV-intensity of 8 W/cm^2. An intensity of this magnitude cured the UV-NIL polymer nearly instantaneously and is, in fact, three orders of magnitude higher than what we use in wafer level imprint.

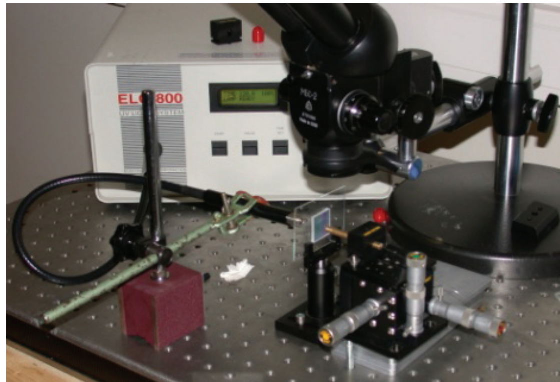

Figure 38. Setup used to fabricate nanopatterned fiber facets.

Using this simple set-up we patterned two sets of fibre facets. We employed a standard single-mode fibre (Corning SMF-28). The first set was patterned using a commercially available blazed grating with 830 lines / mm (Optometrics Corp). The second set of patterns consisted of holes with diameters of 250 nm, arranged in a square lattice with a period of 500 nm. The blazed grating was used in order to study the diffraction efficiency of the imprint. The grating efficiency was defined as the light power of the first-order diffraction mode over the total light power. The efficiency *versus* wavelength is plotted in Figure 39.

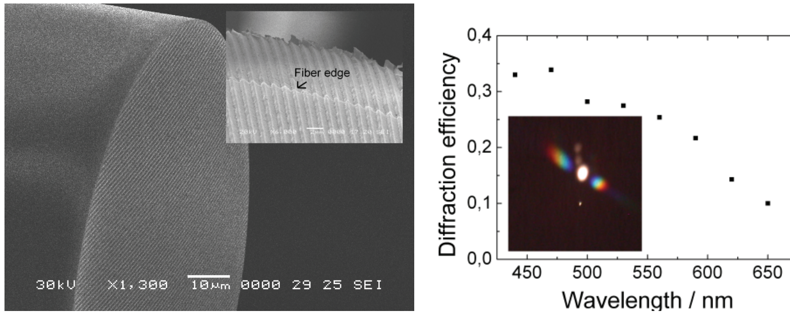

Figure 39. Left panel: SEM image illustrating the facet of the optical fibre with an imprinted blazed grating. Insert: Close up near the fibre edge. On right: Graph of the diffraction efficiency, and an image from the output of the fibre when white light was launched into the fibre.

We studied nanopatterning of the fibre tip. The final imprinted structure exhibited good uniformity. The standard deviation for the diameter of the holes was below 7 nm, as deduced from SEM images taken near the core of the fibre. We think that the main mechanism causing such a deviation was the template itself, which had a standard deviation of this magnitude. The very accurate replica obtained provides clear-cut evidence that UV-NIL can produce flawless sub-wavelength features on a small-area fibre facet. In a recently published article, similar methods were employed by other research groups who fabricated fibre probes for on-wafer optical probing (Scheerlinck *et al*. 2008) and made fibres with integrated surface-enhanced Raman scattering sensors on their facets (Kostovski *et al*. 2009).

6 Conclusion

Nanophotonics is a rapidly growing field of science and engineering with great commercial potential, though we do not fully understand as yet how to scale up a myriad of different applications from the point of view of volume production. The electronics industry has developed its own fabrication methods around optical lithography, but the same methods cannot straightforwardly be applied to the photonics industry. Nanophotonics is, indeed, more fragmented, less standardized, and requires different technical specifications than those used in microelectronics. I predict on good grounds that NIL will play an important role in the commercialization of nanophotonics because it offers excellent cost-effectiveness and needs relatively low capital investment. I dare say that UV-NIL using soft and flexible working stamps, in particular, represents perhaps the best approach in cost-effective production of nano-scale surface reliefs. However, soft UV-NIL, like other new technologies, must be understood thoroughly before it can be applied successfully to device fabrication. I believe that I have addressed in this Thesis some of the key issues which one will encounter when trying to exploit soft UV-NIL.

Remarkably, nanofabrication in the Thesis was possible without owning any template fabrication instruments. This was enabled by outsourcing the template fabrication and by concentrating on pattern replication with NIL. The selected strategy is the same as what has been used successfully for decades in microfabrication with UV-lithography. There is hardly any reason to use self-made photomasks because high-quality photomasks can be obtained at relatively low cost and rapid turn-around time. Obviously, as NIL is a newcomer in the lithography field the situation is not yet as good as with UV-lithography. NIL template vendors often lack redundancy, which sould protect them from instrument failure , delivery times are unreasonably long, and the quality of fabrication is not very well quantified. NIL template vendors should specify, for example, defectivity, line edge roughness, linewidth accuracy, stitching error and registration accuracy for their products, as UV-mask makers do. If quantification is lacking it is very difficult to compare vendors and to justify the differences in pricing.

NIL is not just for volume production. It is important to realize that combining soft and flexible stamps in a mask aligner with freedom from expensive direct write systems, one creates a very accessible nanopatterning concept. Therefore soft UV-NIL, using strategies also applied in this Thesis, makes nanopatterning available to research who have had no opportunity to make their own nanopatterns.

I now proceed to summarize my main results. We developed a NIL-based lithographic process to prepare laterally coupled distributed-feedback lasers at λ = 894.6 nm (in the first place) which are stable over a wide temperature range and have a high side-mode suppression-ratio. We also developed a processing concept that allows efficient coupling between the lasing mode and high injection efficiency. There are still open issues as to these lasers. It is unclear to us how large output power could be launched from such a laterally coupled DFB laser, how reliable this laser is in the long run, and how narrow linewidths could be achieved. It is also somewhat unclear to which extent any lateral grating placed alongside the waveguide couples to the optical cavity through pure index-coupling, and what role the gain coupling might be playing. Our latest results are related to a laterally coupled DFB laser emitting at λ = 1945 nm, made of an antimonide containing heterostructure (unpublished). This result was achieved by developing high-quality dry-etching (Section 3). In the non-distant future, we shall demonstrate a DFB laser at the fibre optical wavelength of 1310 nm using a first-order grating to yield strong enough coupling with a short cavity, thus enabling a high modulation bandwidth for data transfer.

Accurately positioned quantum dots by means of NIL is another noteworthy direction of our work. This work may well produce novel gain materials and novel devices, but we must bear in mind that there exists a long road from reasonable SEM images and photoluminescence to state-of-the-art devices which require flawless quantum dots over a large area.

Our approach to fabricate nanoperforated sieves for particle filtering should provide ready solutions for novel filters. If a further reduction in perforation diameter were necessary, it could be made at the expense of pattern density (*via* ALD size tuning), or at the expense of the effective area of the membrane (because smaller perforations require a thinner membrane and more mechanical support). Future development would make it possible to fabricate higher aspect ratio perforations than what we have made which, in turn, would further push the boundaries of the

device geometry. Our results obtained on SOI wafers were encouraging, but the development was hindered by non-uniformity of the device layer and undercutting caused by cryo-etching. I suggest that these obstacles could be overcome by using Boch etching which would enable strong passivation of pattern side walls and, therefore, eliminate undercutting that is induced by non-uniformity. Another way to improve the sieve is to analyze the relationship between the layer thickness, area, and durability of the membrane and to come up with new design rules that relate the device geometry to device performance features.

We also demonstrated novel approaches for interaction of laser light exiting or entering an optical fiber, using NIL-made nanopatterning. In order to continue this research we would like to find a "killer" application. One could imagine that the miniature size of these functional fibers would allow their use as probes or, alternatively, they could be suitable for decorative elements because of their very low fabrication costs.

7 References

Abe H., Ayling S. G., Marsh J. H., De La Rue R. M., and Roberts J. S. (1995), Single-mode operation of a surface grating distributed feedback GaAs-AlGaAs laser with variable-width waveguide, *IEEE Photon Technol. Lett.*, Volume 7, Issue 5, pp. 452–454

Allsop T., Neal R., Rehman S., Webb D. J., Mapps D. and Bennion I. (2007), Generation of infrared surface plasmon resonances with high refractive index sensitivity utilizing tilted fiber Bragg gratings, A*pplied optics,* Volume 46, Issue 22, pp. 5456-5460

Austin M. D., Zhang W., Ge H., Wasserman D., Lyon S. A. and Chou S. Y. (2005), 6 nm half-pitch lines and 0.04 μm^2 static random access memory patterns by nanoimprint lithography, *Nanotechnology,* Volume **16,** pp. 1058-1061

ASML (2009), ASML, TWINSCAN™ NXT:1950i specifications

Babin S., Bay K. and S. Okulovsky (2005), Prediction of etch profile and CD variation due to dry etch using TRAVIT software tool, *Spie proceedings 5853*, *Photomask and Next-Generation Lithography Mask Technology XII*, pp.66-73

Beck M., Graczyk M., Maximov I., Sarwe E. -L., Ling T. G. I., Keil M. and Montelius L. (2002), Improving stamps for 10 nm level wafer scale nanoimprint lithography, *Microelectronic Engineering*, Volume **61–62**, pp. 441 –448

Bender M., Plachetka U., Ran J., Fuchs A., Vratzov B., Kurz H., Glinsner T. and Lindner F., High resolution lithography with PDMS molds, *J. Vac. Sci. Technol. B,* Volume 22, Issue 6, pp. 3229-3232

Bietscha A. and Michel B. (2000), Conformal contact and pattern stability of stamps used for soft lithography, *J. Appl. Phys.,* Volume 88, Number 7, pp. 4310-4318

Bird R. B., Armstrong R. C. and Hassager O. (1977), *Dynamics of Polymer Liquids*, *Fluid Mechanics*, Volume 1, John Wiley & Sons, 1977

Brooks C., Schmid G., Miller M., LaBrake D., Hofemann P., Resnick D., Sreenivasan S.V. (2009), Patterned Media Using Step and Flash Imprint Lithography, SPIE Advaned Lithography Conf., Alternative Lithographic Technologies, *Proc. of SPIE,* Volume 7271, , San Jose, USA

Britt D. W. and Hlady V. (1996), An AFM Study of the Effects of Silanization Temperature, Hydration, and Annealing on the Nucleation and Aggregation of Condensed OTS Domains on Mica, *Journal of Colloid and Interface Science*, Volume 178, Issue 2, pp. 775-784

Brzoska J. B., Azouz I. B., and Rondelez F. (1994), Silanization of Solid Substrates: A Step Toward Reproducibility, *Langmuir*, ***10*** (11), pp. 4367–4373

Chang J.-H., Cheng F.-S., Chao C.-C., Weng Y.-C., Yanga S.-Y. and Wang L. A. (2005), Direct imprinting using soft mold and gas pressure for large area and curved surfaces, *J. Vac. Sci. Technol. A.,* Volume 23, Issue 6, pp. 1687-1690

Cheng J. and Dutta N. K. (2000), Vertical-cavity surface-emitting lasers: technology and applications in book series "Optoelectronic properties of semiconductors and superlattices" Volume 10

Cheong W.-S. (2003), Optimization of Selective Epitaxial Growth of Silicon in LPCVD, *ETRI Journal*, Volume 25, Number 6, pp. 503-509

Cho Y., Kwon S., Seo J.-W., Kim J.-G., Cho J.-W., Park J.-W., Kim H. and Lee S. (2009), Development of large area nano imprint technology by step and repeat process and pattern stitching technique, *Microelectronic Engineering*, Volume 86, pp. 2417–2422

Choi K.M. and Rogers J.A. (2003), A Photocurable Poly(dimethylsiloxane) Chemistry Designed for Soft Lithographic Molding and Printing in the Nanometer Regime, *J. Am. Chem. Soc.* Volume 125, Issue 14, pp. 4060-4061

Chou S. Y., Krauss P. R., and Renstrom P. J. (1995) Imprint of sub-25 nm vias and trenches in polymers, *Appl. Phys. Lett.*, Volume 67, pp. 3114-3116

Chou S. Y., Krauss P. R., Zhang W.,Guo L. and Zhuang L. (1997), Sub-10nm imprint lithography and applications, *J. Vac. Sci. Technology B*, Volume 15, pp. 2897-2904

Costner E. A., Lin M. W., Jen W.-L. and Willson, C. G. (2009), Nanoimprint Lithography Materials Development for Semiconductor Device Fabrication, Annual Review of Materials Research, Volume 39, Number 1, pp. 155-180

Dylewicz R., Bryce C., Sorel M., and De La Rue R. (2009), High Aspect Ratio Inductively Coupled Plasma (ICP) Etching of InP/InGaAsP/AlGaInAs Using Cl_2/Ar/N_2 Gas Mixture, *CLEO Europe 2009*, Munich, 14-19 June 2009, Poster CE.P.31 MON

Dow Corning (2009), Sylgard® 184 silicone elastomer kit, product datasheets, electronics

Fiedler F., Schlachetzki A. and Klein G. (1982), Material-selective etching of InP and an InGaAsP alloy, Journal of Materials Science, Volume 17, Number 10, pp. 2911-2918

French R. H., Sewell H., Yang M. K., Peng S., McCafferty D. C., Qiu W., Wheland R. C., Lemon M. F., Markoya L. and Crawford M. K. (2005), Imaging of 32-nm 1:1 lines and spaces using 193-nm immersion interference lithography with second-generation immersion fluids to achieve a numerical aperture of 1.5 and a k_1 of 0.25, *Journal of Micro/Nanolithography, MEMS, and MOEMS,* Volume 4, Issue 3, 031103

Fuard D., Tzvetkova-Chevolleau T., Decossas S., Tracqui P. and Schiavone P. (2008), Optimization of poly-di-methyl-siloxane (PDMS) substrates for studying cellular adhesion and motility, *Microelectronic Engineering*, Volume 85, Issue 5-6, pp. 1289-1293

Gelest Inc. (2009), Silicone coatings, encapsulats, gels. Performance property guide for Dielectric, Optical, Thermal and Mechanical applications

Giannini G., Mastrogiacomo L., Cabrini S., Gerardino A., Nottola A., Foglietti V. and Cianci E. (2000), Microfabrication of diffractive optical elements onto the active region of optical fiber termination, in *Proc. MICRO tec.2000.-VDE World Microtechnologies Congress*, volume 2, pp. 695-697, Berlin, Germany

Glinsner T., Plachetka U., Matthias T., Wimplinger M. and Lindner P. (2007), Soft UV-based nanoimprint lithography for large-area imprinting applications, Emerging Lithographic Technologies XI. *Proceedings of the SPIE*, Volume 6517, pp. 651718

Golka S., Pflügl C., Schrenk W., and Strasser G. (2005), Quantum cascade lasers with lateral double-sided distributed feedback grating, *Appl. Phys. Lett.*, Volume 86, 111103

Gourgon C., Perret C., Tallal J., Lazzarino F., Landis S., Joubert O. and Pelzer R. (2005), Uniformity across 200 mm silicon wafers printed by nanoimprint lithography, *Journal of Physics D: Applied Physics,* Volume 38, Number 1, pp. 70-73

Gregus J. A., Vernon M. F. , Gottscho R. A., Scheller G. R., Hobson W. S., Opila R. L. and Yoon E. (1993), Low-temperature plasma etching of GaAs, AlGaAs, and AlAs, *Plasma Chemistry and Plasma Processing*, Volume 13, Issue 3, pp. 521-537

Guo L. J. (2004), Recent progress in nanoimprint technology and its applications, *J. Phys. D: Appl. Phys.* Volume 37, pp. R123–R141

Guo L. J. (2007), Nanoimprint Lithography: Methods and Material Requirements, *Adv. Mater.*, Volume 19, pp. 495–513

Hancer M. (2008), The effect of humidity on the stability of octadecyltrichlorosilane for the self-assembled monolayer coating applications, *Progress in Organic Coatings*, Volume 63, Issue 4, pp. 395-398

Hanumegowda N. M., Stica C. J., Patel B. C., White I., and Fana X. (2005), Refractometric sensors based on microsphere resonators, Appl. Phys. Lett. 87, pp. 201107

Henry C. H. (1985), Performance of distributed feedback lasers designed to favor the energy gap mode, *IEEE J. Quantum Electron.*, Volume 21, pp. 1913-1918

Hoffmann T. (2002), Viscoelastic Properties of Polymers, Chapter 3 in book *Alternative lithography, unleashing the potential of nanotechnology*, in series Nanostructure science and thechnology, Edited by Clivia M. Sotomyor Torres, Kluwer Academic / Plenum Publishers, pp. 25-46

Houle F. A., Rettner C. T., Miller D. C., and Sooriyakumaran R. (2007), Antiadhesion considerations for UV nanoimprint lithography, Appl. Phys. Lett., Volume 90, 213103

Hua F., Sun Y., Gaur A., Meitl M. A., Bilhaut L., Rotkina L., Wang J., Geil P., Shim M. and Rogers J. A. (2004), Polymer Imprint Lithography with Molecular-Scale Resolution, *Nano Letters*, Volume 4, Issue 12, pp. 2467-2471

Kamp M., Hofmann J., Schäfer F., Reinhard M., Fischer M., Bleuel T., Reithmaier J. P. and Forchel A. (2001), Lateral coupling – a material independent way to complex coupled DFB lasers, *Optical Materials,* Volume 17, Issues 1-2, pp. 19-25

Kang H., Lee J., Park J. and Lee H. H. (2006), An improved method of preparing composite poly(dimethylsiloxane) moulds, *Nanotechnology*, Volume 17, pp. 197–200

Kim J.G., Takama N. Blech V. and Kim B.J. (2004), Nano Scale Surface Patterning by Micro Contact Printing using a Novel Type of PDMS Stamp, *Proceedings of The 2nd International Symposium on Nanomanufacturing (ISNM2004)*, pp. 308-311, 2004

Kim K-d., Jeong J-h., Sim Y.-s. and Lee E.-s. (2006), Minimization of residual layer thickness by using the optimized dispensing method in S-FILTM process, *Microelectronic Engineering,* Volume 83, Issues 4-9, pp. 847-850

Klukowska A., Kolander A., Bergmair I., Mühlberger M., Leichtfried H., Reuther F., Grützner G. and Schöftner R. (2009), Novel transparent hybrid polymer working stamp for UV-imprinting, Microelectronic Engineering, Volume 86, Issue 4-6, pp. 697-699

Komatsubara S. (1984), Method of manufacturing stamper for information storage discs, US patent 4,482,511.

Kontio J.M, Husu H, Simonen J., Huttunen M.J, Tommila J., Pessa M., and Kauranen M. (2009a), Nanoimprint fabrication of gold nanocones with ~10 nm tips for enhanced optical interactions, Optics Letters, Volume 34, pp. 1979–1981

Kontio J.M., Simonen J., Tommila J., and Pessa M. (2009b), Arrays of metallic nanocones fabricated by UV-nanoimprint lithography, Article in press, *Microelectronic Engineering*

Koo N., Bender M., Plachetka U., Fuchs A., Wahlbrink T., Bolten J. and Kurz H. (2007), Improved mold fabrication for the definition of high quality nanopatterns by Soft UV-Nanoimprint lithography using diluted PDMS material, *Microelectronic Engineering*, Volume 84, pp. 904-908

Kostovski G., White D.J., Mitchell A., Austin M.W. and Stoddart P.R. (2009), Nanoimprinted optical fibres: Biotemplated nanostructures for SERS sensing, Biosensors and Bioelectronics, Volume 24, Issue 5, pp. 1531-1535

Lan H., Ding Y., Liu H., Que Y., Tao W., Li H. and Lu B., Mold deformation in soft UV-nanoimprint lithography (2009), Volume 52, Number 2, pp. 294-302

Lazzarino F., Gourgon C., Schiavone P. and Perret C. (2004), Mold deformation in nanoimprint lithography, *J. Vac. Sci. Technol. B,* Volume 22, Issue 6, pp. 3318-3322

Lee P.-S., Lee O.-J., Hwang S.-K., Jung S.-H., Jee S.-E., and Lee K.-H. (2005), Vertically Aligned Nanopillar Arrays with Hard Skins Using Anodic Aluminum Oxide for Nano Imprint Lithography, *Chem. Mater.*, Volume 17, pp. 6181-6185

Li M., Chen L., Zhang W. and Chou S. Y. (2003), Pattern transfer fidelity of nanoimprint lithography on six-inch wafers, *Nanotechnolgy*, Volume 14, pp. 33-36

Liang X., Tan H., Fu Z. and Chou S. Y. (2007), Air bubble formation and dissolution in dispensing nanoimprint lithography, *Nanotechnology,* Volume 18, Number 2, pp. 025303

Levola T. and Laakkonen P. (2007), Replicated slanted gratings with a high refractive index material for in and outcoupling of light, *Optics Express*, Volume 15, pp. 2067-2074

Liang W., Huang Y., Xu Y., Lee R. K. and Yariv A. (2005), Highly sensitive fiber Bragg grating refractive index sensors, *Appl. Phys. Lett.,* Volume 86, pp. 151122

Lin C., Grau M., Dier O. and Amann M.-C. (2004), Low threshold room-temperature continuous-wave operation of 2.24–3.04 µm GaInAsSb/AlGaAsSb quantum-well lasers, *Appl. Phys. Lett.,* Volume 84, pp. 5088

Lyutetskii A. V., Pikhtin N. A., Slipchenko S. O., Sokolova Z. N., Fetisova N. V., Leshko Yu. A., V. Shamakhov V., Andreev A. Yu., Golikova E. G., Ryaboshtan Yu. A. and Tarasov I. S. (2003), 1.7–1.8 µm Diode lasers based on quantum-well InGaAsP/InP heterostructures, *Semiconductors*, Volume 37, Issue 11, pp. 1356–1362

Mapper Lithography (2009), Press Release 2008, http://www.mapperlithography.com/, Checked 1.6.2009

Mckee A., Mclean C. J., Lullo G., Bryce A. C., De La Rue R. M., Marsh J. H., Button C. C. (1997), Monolithic integration in InGaAs-InGaAsP multiple-quantum-well structures using laser intermixing, *IEEE journal of quantum electronics*, Volume 33, Issue 1, pp. 45-55

McClelland G. M., Rettner C. T., Hart M.W., Carter K.R., Sanchez M. I., Best M. E. and Terris B.D. (2005), Contact mechanics of a flexible imprinter for photocured nanoimprint lithography, Tribology Letters, Volume 19, Number 1, pp. 59-63

McCord M. and Brooks M. (1997), Electron Beam Lithography, Chapter 2 in book Handbook of Microlithography, Micromachining and Microfabrication, Volume 1: Microlithography

Newell T., Wu X., Gray A. L., Dorato S., Lee H. and Lester, L. F., The effect of increased valence band offset on the operation of 2 µm GaInAsSb-AlGaAsSb lasers, *IEEE Photonics Technology Letters*, Volume 11, Issue 1, pp. 30 – 32

Micro Resist Technology (2009a), Preliminary process guidelines, contact person: Anna Klukowska

Micro Resist Technology (2009b), Ormocer®s (hybrid polymers) for micro optics, product flyer

Miller M., Brooks C., Lentz D., Doyle G., Resnick D., Labrake D. (2008), Step and Flash Imprint Process Integration Techniques for Photonic Crystal Patterning : Template Replication through Wafer Patterning Irrespective of Tone, *Proceedings of SPIE*, ISBN 978-0-8194-7058-4, Volume 6883, pp. 68830D.1-68830D.9

Miller, L.M., Verdeyen, J.T., Coleman, J.J., Bryan, R.P., Alwan, J.J., Beernink, K.J., Hughes, J.S. and Cockerill, T.M. (1991), A distributed feedback ridge waveguide quantum well heterostructure laser, *IEEE Photonics Technology Letters*, Volume 3, Number 1, pp. 6-8

Nature Photonics Issue “Antennas of Light” (2008), Nature Photonics, Volume 4, Issue 199

Magnusson R. and Wang S. S. (1992), New principle for optical filters, *Appl. Phys. Lett.,* Volume 61, pp. 1022

Obducat (2010), Web site www.obducat.com/ inspected 14.4.2010

Ohta T., Hennesey M., Strand D., Jablonsky D., Walton B., and Clark B. (2007), High Quality Film Nanoimprint Technology for Blu-Ray Disc (BD) Media, *IEEE Transactions on magnetics*, Volume 43, Number 2, pp. 836-839

Park Y. B.,. Yoon I. Y, Ryu H. H. and Lee W. G. (2001), Pattern density and deposition profile effects on oxide chemical-mechanical polishing and chip-level modeling, *Journal of Electronic Materials*, Volume 30, Number 12, pp. 1560-1568

Pessa, M. Peng, C.S. Jouhti, T. Pavelescu, E.-M. Li, W. Karirinne, S. Liu, H. Okhotnikov, O. (2003), Towards high-performance nitride lasers at 1.3 µm and beyond, *IEE Proceedings of Optoelectronics*, Volume 150 Issue 1, pp. 12- 21

Petric P., Bevis C., Brodie A., Carroll A., Cheung A., Grella L., McCord M., Percy H., Standiford K., and Zywno M. (2009) REBL Nanowriter: Reflective Electron Beam Lithography, Advanced Lithography, *Proc. of SPIE Vol.* 7271 727107-1, San Jose, USA

Perret C., Gourgon C., Lazzarino F., Tallal J., Landis S. and Pelzer R. (2004), Characterization of 8-in. wafers printed by nanoimprint lithography, *Microelectronic Engineering* Volume 73-74, pp. 172-177

Plachetka U., Bender M., Fuchs A., Vratzov B., Glinsner T., Lindner F. and Kurz H. (2004), Wafer scale patterning by soft UV-Nanoimprint Lithography, *Microelectronic Engineering* Volumes 73-74, pp. 167-171

Pozzi F., De La Rue R. M., and Sorel M. (2006). Dual-Wavelength InAlGaAs–InP Laterally Coupled Distributed Feedback Laser, *IEEE Photon Technol. Lett.*, Volume 18, Issue 24, pp. 2563-2565

Ross N., Wissen M., Glinsner T. and Scheer (2003), Impact of vacuum environment on the hot embossing process, *Proc. SPIE*, Volume 5037, pp. 211-218

Rowland H. D., Sun A. S., Schunk P. R. and King W. P. (2005), Impact of polymer film thickness and cavity size on polymer flow during embossing: toward process design rules for nanoimprint lithography, *Journal of Micromechanics and Microengineering*, Volume 15, Number 12, pp. 2414

Sainiemi, L., Viheriälä J., Laukkanen, J., Niemi T. and Franssila S. (2009c), Fabrication of nanoperforated silicon membranes with tunable sized high aspect ratio holes, *The 15th International Conference on Solid-State Sensors, Actuators and Microsystems*, Denver, Colorado, USA, June 21 - 25, 2009

Scheerlinck S., Taillaert D., Van Thourhout D., Baets R. (2008), Flexible metal grating based optical fiber probe for photonic integrated circuits, *Appl. Phys. Lett.*, Volume 92, 031104

Schiappelli F., Prasciolu M., Cojoc D., Cabrini S. and Di Fabrizio E. (2003), Design and fabrication of lenses on the top of an optical fiber for efficient fiber-to-waveguide coupling by means of Focus Ion Beam (FIB) lithography," in *Dig. of Papers Microprocesses and Nanotechnology*, pp. 166-7., Int. Microprocesses and Nanotechnol. Conf., Tokyo

Schift H. and Heyderman L. J. (2002), Squueze Flow in Hot Embossing of Thin Films, Chapter 4 in book *Alternative lithography, unleashing the potential of nanotechnology*, in series Nanostructure science and thechnology, Edited by Clivia M. Sotomyor Torres, Kluwer Academic / Plenum Publishers, pp. 25-46

Schift H. (2009), Nanoimprint lithography: An old story in modern times? A review, *J. Vac. Sci. Technol. B*, Volume 26, Issue 2, pp. 458-480

Schmid H. and Michel B. (2000), Siloxane Polymers for High-Resolution, High-Accuracy Soft Lithography. *Macromolecules*, Volume 33, pp. 3042-3049

Schuster C., Reuther F., Kolander A., Gruetzner G. (2009), mr-NIL 6000LT – Epoxy-based curing resist for combined thermal and UV nanoimprint lithography below 50 °C , *Microelectronic Engineering,* Volume 86, Issue 4-6, Pages 722-725

Shiraishi K., Ohnuki H., Hiraguri N., Matsumura K., Ohishi I., Morichi H. and Kazami H. (1997), *J. Lightw. Technol.*, Volume 15, pp. 356-363

Sorel M., Strain M. and Mezosi G. (2008). Semiconductor ring lasers for ultra fast all-optical digital processing, European Semiconductor Laser Workshop 2008, Eindhoven, Netherlands, 9th – 20th September

Solak H. H., Ekinci Y., Käser P. and Park S. (2007), Photon-beam lithography reaches 12.5 nm half-pitch resolution, *J. Vac. Sci. Technol. B,* Volume 25, Issue 1, pp. 91-95

Sotomayor Torres C. L. (2003), Alternative Lithography Unleashing the potentials of nanotechnology, Book in series Nanostructure science and technology, Kluwer Academic / Plenum Publishers

Spindt C.A. (1968), A Thin-Film Field-Emission Cathode, *Journal of Applied Physics*, Volume 39, pp. 3504

Sreenivasan S.V., Schimaker P., Mokaberi B., Choi J., Perez J., Truskett V., Xu F., Lu X. (2009), Recent Developments in UV Nanoimprint Stepper Technology for Sub-30nm Half-Pitch Lithography, SPIE Advaned Lithography Conf., *Proc. of SPIE* Vol. 7271, San Jose, USA, February, 2009

Sumpf B., Zorn M., Staske R., Fricke J., Ressel P., Erbert G., Weyers M. and Tränkle G. (2006), 5-W reliable operation over 2000 h of 5-mm-wide 650-nm AlGaInP-GaInP-AlGaAs laser bars with asymmetric cladding layers, *IEEE photonics technology letters*, Volume 18, Issue 17-20, pp. 1955-1957

Sumitomo, (2009) Sumitomo Electric, GaAs and InP wafer flatness specifications, 19.1.2009. "http://www.sei.co.jp/sc/products_e/gaas/pdf/materials07_08.pdf"

Sun X., Zhuang L., Zhang W. and Chou S. Y. (1998), Multilayer resist methods for nanoimprint lithography on nonflat surfaces, *J. Vac. Sci. Technol. B,* Volume 16, pp. 3922-3925

Suss Microtech, (2009), Spesfications for automatic and semiautomatic mask aligners

Tandon A., Bour D. P., Chang Y.-L.; Lin C. K., Corzine S. W. and Tan M. R. (2004), Low-threshold, high-T0 and high-efficiency 1300nm and 1500nm lasers with AlInGaAs active region grown by MOCVD, *Physics and Simulation of Optoelectronic Devices XII,* Proceedings of the SPIE, Volume 5349, pp. 206-217

Technology review (2003), 10 Emerging Technologies That Will Change the World, *Technology review*, Issue 38, Ferbruary 2003

Telkkälä J., Laakso A., Viheriälä J., Karinen J., Leinonen T., Toikkanen L., Dumitrescu M. and Pessa M. (2009), Laterally-coupled distributed feedback laser diodes emitting at 894 nm fabricated by using nanoimprint lithography, *3rd ESA International Workshop on Optical Atomic Clocks*, 14 - 16 October 2009, ESA-ESRIN, Frascati, Rome, Italy

Tolstikhin, V.I. Watson, C.D. Pimenov, K. Moore, R. Logvin, Y. Wu, F. (2009), Laterally Coupled DFB Lasers for One-Step Growth Photonic Integrated Circuits in InP, *IEEE Photonics Technology Letters,V*olume 21, Number 10, pp.621-623

Tukiainen A., Viheriälä J., Niemi T., Rytkönen T., Kontio J. and Pessa M. (2006), Selective growth Experiments on Gallium arsenide (100) surfaces patterned using UV-nanoimprint lithography, *Microelectrics Journal*, Volume 37, Issue 12, pp. 1477-1480

Tukiainen A., Aho A., Tommila J., Ahorinta R., Viheriälä J., Dumitrescu M. and Pessa M. (2009), Growth of InAs Quantum Dots on Selectively Grown GaAs Nanopyramids on Nanoimprint-Patterned n-GaAs(100) Substrates, PALS 2009 - The 4th Finnish-Russian Photonics and Laser Symposium, May 24 - 27, Tampere, Finland

Vieu C., Carcenac F., Pépin A., Chen Y., Mejias M., Lebib A., Manin-Ferlazzo L., Couraud L. and Launois H. (2000), Electron beam lithography: resolution limits and applications, *Applied Surface Science,* Volume 164, pp. 111-117

Viheriälä J., Niemi T., Kontio J., Rytkönen T. and Pessa M. (2007) Fabrication of surface reliefs on facets of singlemode optical fibres using nanoimprint lithography, *Electronics letters,* Volume 43, Issue 3, pp. 150-152

Viheriälä J., Rytkönen T., Niemi T. and Pessa M. (2008). Narrow linewidth templates for nanoimprint lithography utilizing conformal deposition, *Nanotechnology, Volume* 19, 015302

Viheriälä J., Tommila J., Leinonen T., Dumitrescu M., Toikkanen L., Niemi T. and Pessa M. (2009), Applications of UV-nanoimprint soft stamps in fabrication of single-frequency diode lasers, *Microelectronic Engineering*, Volume 86, Issue 3, pp. 321-324

Viheriälä J., Viljanen M.-R., Kontio J., Leinonen T., Tommila J., Dumitrescu M., Niemi T. and Pessa M. (2009b), Soft Stamp UV-Nanoimprint Lithography for Fabrication of Laser diodes, *Journal of Micro/Nanolithography, MEMS, and MOEMS*, vol. 8, 033004

Viheriälä J., Niemi T., Laukkanen J., Karjalainen M. and Pessa M. (2009c), *Microelectronics engineering*, Volume 87, Number 5 - 8, pp. 1620-1622

Wieland M.J., de Boer G., ten Berge G.F., Jager R., van de Peut T., Peijster J.J.M., Slot E., Steenbrink S.W.H.K., Teepen T.F., van Veen A.H.V., Kampherbeek B.J. (2009) MAPPER: High throughput maskless lithography, Alternative Lithographic Technologies, *Proc. of SPIE* Vol. 7271, 72710O, San Jose, USA

Williams B. S., Kumar S., John Q. H. and Reno L. (2005), Distributed-feedback terahertz quantum-cascade lasers with laterally corrugated metal waveguides, *Optics Letters*, volume 30, Issue 21, pp. 2909-2911

Yeh S.-M., Lu Y.-K., Huang S.-Y., Lin H.-H., Hsieh C.-H., and Cheng W.-H (2004) A novel scheme of lensed fiber employing a quadrangular-pyramid-shaped fiber endface for coupling between high-power laser diodes and single-mode fibers, *J. Lightw. Technol.*, Volume 22, Issue 5, pp. 1374-1379

Yu Z., Wu W., Jung G.-Y., Olynick D. L., Straznicky J., Li X., Li Z., Tong W. M., Liddle J. A., Wang S.-Y. and Williams R. S. (2006) "Fabrication of 30 nm pitch imprint moulds by frequency doubling for nanowire arrays" *Nanotechnology*, Volume 17, pp. 4956–4961

Zhou W., Zhang J., Liu Y., Li X., Niu X., Song Z., Min G., Wan Y.-Z., Shi L. and Feng S. (2008), Characterization of anti-adhesive self-assembled monolayer for nanoimprint lithography, *Applied Surface Science*, Volume 255, Issue 5, pp. 2885-2889

Publication 1

Jukka Viheriälä, Tuomo Rytkönen, Tapio Niemi and Markus Pessa (2008), Narrow linewidth templates for nanoimprint lithography utilizing conformal deposition, *Nanotechnology* , Volume 19, 015302, (7pp)

© Institute of Physics and IOP Publishing Limited 2008. Reproduced with permission.

Publication 2

Jukka Viheriälä, Tapio Niemi, Juha Kontio, Tuomo Rytkönen and Markus Pessa (2007), Fabrication of surface reliefs on facets of single-mode-fibers using nanoimprint lithography, *Electronic Letters*, Volume 43, Number 3, pp. 150-152

© IEEE 2007. Reproduced with permission.

Publication 3

Jukka Viheriala, Juha Tommila, Tomi Leinonen, Michail Dumitrescu, Lauri Toikkanen, Tapio Niemi and Markus Pessa (2009), Applications of UV-nanoimprint soft stamps in fabrication of single-frequency diode lasers, *Microelectronic Engineering*, Volume 86, Number 3, pp. 321-324

© 2009 Elsevier B.V. Reproduced with permission.

Appendix 4

Publication 4

Jukka Viheriälä, Milla-Riina Viljanen, Juha Kontio, Tomi Leinonen, Juha Tommila, Mihail Dumitrescu, Tapio Niemi and Markus Pessa (2009), Soft Stamp UV-Nanoimprint Lithography for Fabrication of Laser Diodes, *Journal of Micro/Nanolithography* MEMS, and MOEM, Volume 8, 033004

© 2009 Society of Photo-Optical Instrumentation Engineers. Reproduced with permission.

Publication 5

Lauri Sainiemi, **Jukka Viheriala**, Janne Laukkanen, Tapio Niemi and Sami Franssila (2009), Fabrication Of Silicon Membranes With Tunable Sized High Aspect Ratio Nanoperforations, Technical Digest of Transduces 2009, Paper M3.P045

©2009 IEEE. Reproduced with permission.

Publication 6

Jukka Viheriälä, Tapio Niemi, Janne Laukkanen, Maija Karjalainen and Markus Pessa, Large area Nanoperforated SiN membranes for Optical and Mechanical Filtering (2010), *Microelectronics Engineering,* Volume 87, Number 5 - 8, pp. 1620-1622

© 2009 Elsevier B.V. Reproduced with permission.

Publication 7

Antti Tukiainen, **Jukka Viheriälä**, Tapio Niemi, Tuomo Rytkönen, Juha Kontio and Markus Pessa (2006), Selective growth Experiments on Gallium arsenide (100) surfaces patterned using UV-nanoimprint lithography, *Microelectrics Journal*, Volume 37, Issue 12, pp. 1477-1480

© 2006 Elsevier Ltd. Reproduced with permission.